Noncovalent Immobilization of Electrocatalysts on Carbon Electrodes via a Pyrenyl Ligand

Thesis by
Ayush Gupta

In Partial Fulfillment of the Requirements for
the degree of
Bachelor of Science

CALIFORNIA INSTITUTE OF TECHNOLOGY
Pasadena, California

2016
(Submitted June 3, 2016)

ACKNOWLEDGEMENTS

I would like to first express my deepest thanks to Harry B. Gray for allowing me to work in his group and enable me to grow as a chemist. I was able to first meet Harry during the summer meeting as a high school student. His enthusiastic and welcoming attitude convinced me to attend Caltech and study chemistry. Ever since joining the Solar Army, I have had countless opportunities to explore ideas and concepts that helped me grow both as a scientist and as a person. My work has inspired me to continue studying inorganic chemistry in graduate school at the University of Chicago.

I would also like to greatly thank James D. Blakemore who has been my postdoctoral mentor for the past three years. I started working with James as a freshman. We started off a bit slow, but as I got accustomed to the lab, he gave me more freedom to problem solve and propose new ideas on ongoing projects. Even while preparing to go to the University of Kansas, James has always been willing to give a helpful word or two of advice. Working with James has been a great experience and I look forward to potential collaborations with him in the future.

Working with various members of the Gray Group over the past three years has been very helpful. I am very grateful to the help given by Bruce Brunschwig and Jay Winkler for offering help or advice when needed. Other members of the group that I would like to thank for providing help, useful discussion, or ideas are Peter Agbo, Jeffrey Warren, Oliver Shafaat, Brian Sanders, Bryan Hunter, Chris Roske, David VanderVelde for NMR, and David Lacy for GCMS.

My work has been supported by the Caltech SURF program, the National Science Foundation (NSF) Center for Chemical Innovation in Solar Fuels, and the Resnick Sustainability Institute at Caltech The work on X-ray photoelectron spectroscopy was supported by a California Energy Commission contract

ABSTRACT

There are many problems that need to be overcome if solar energy is to be viable on a global scale. Photons must be harvested and stored in a usable to allow efficient use of energy throughout the day. The functionalization of electrode surfaces with molecular catalysts is an attractive route for assembling (photo)electrochemical devices that convert renewable energy into chemical fuels. This work focuses on one method of noncovalently attaching molecular catalysts to graphitic surfaces.

The first part describes the synthesis of a pyrene-appended bipyridine ligand that serves as the linker between the catalysts and the surface. Using this ligand, a rhodium proton-reduction catalyst and a rhenium CO_2-reduction catalyst were synthesized in order to study the electrochemistry of the surface-attached species. Electrochemical and spectroscopic analysis confirm catalyst immobilization and electrocatalytically active assemblies. Bulk electrolysis of the surface-attached complexes confirm catalytic turnover formation of H_2 for the rhodium complex and CO for the rhenium complex.

The second part describes three new complexes utilizing the same pyrene-appended bipyridine ligand. These are [Ru(P)(4,4'-dimethyl-2,2'-bipyridine)$_2$]Cl_2, [Cp*Ir(**P**)Cl]Cl, and [Mn(**P**)$(CO)_3$Br]. Once again, spectroscopic and electrochemical analyses confirmed successful immobilization of these complexes on high surface area carbon electrodes. The iridium complex was found to be unstable with respect to redox cycling due to ligand exchange. The ruthenium complex exhibited very high stability over long periods of redox cycling. The manganese complex was found to catalytically produce CO during bulk electrolysis.

TABLE OF CONTENTS

List of Figures and Schemes

NOMENCLATURE

Bpy. 2,2'-bipyridine

CV. Cyclic Voltammetry

Cp*. 1,2,3,4,5-pentamethylcyclopenta-1,3-diene

DCM. Dichloromethane

DMF. Dimethylformamide

Fc. Ferrocene

GC. Gas chromatograph

HOPG. Highly oriented pyrolytic graphite

MeCN. Acetonitrile

TFE. 2,2,2-Trifluoroethanol

Tosic Acid. *p*-toluenesulfonic acid

XPS. X-ray photoelectron spectroscopy

Chapter 1

Development and Study of a Novel Pyrene-Appended Ligand in a Rhodium and Rhenium Complexes

Introduction

The ever-increasing global need for energy encourages development of clean, renewable sources. Among all renewables, the sun is the only one solely sufficient to meet our current and future energy needs. Many methods for harnessing solar energy are known (e.g., photovoltaic cells, solar water heaters), but new efficient and scalable storage methods must be developed to make solar energy utilization possible on the global scale.[i] One of the most attractive schemes along this line is storage of solar energy in chemical bonds (i.e., solar fuels). Water splitting to produce hydrogen and oxygen is perhaps the most well-known chemistry in this regard, since it produces hydrogen (a fuel) and only oxygen gas as a byproduct.

The Gray group has been working for many years on preparing photoactive materials and well-defined catalysts for hydrogen generation, since the uncatalyzed pathways for hydrogen production are inefficient. Eventually, our group's research will allow assembly of nanostructured materials that efficiently harvest light, separate charges, and channel those charges into productive fuel-forming reactions.[ii]

Little work has focused on attaching homogeneous catalysts to electrode surfaces, but it remains an important research focus since the electrode/electrolyte junction is a key feature of most schemes for solar-fuel production. The functionalization of electrode surfaces with molecular catalysts is an attractive route for assembling (photo)electrochemical devices that convert renewable energy into chemical fuels. [iii,] In such systems, immobilized metal complexes are envisioned to facilitate the reduction of abundant feedstocks (e.g., water, carbon dioxide) to fuels. Inorganic and organometallic complexes have attracted major attention in homogeneous systems, because their mechanisms should be molecular in nature and therefore tunable and selective for the desired reactions, such as the reduction of H^+ to H_2 or CO_2 to liquid fuels. However,

transitioning molecular catalysts from homogeneous solutions to surface-attached systems that are more suitable for device fabrication remains a challenge. [iv] Routes for catalyst immobilization are often not widely applicable, and require harsh conditions that can damage the catalytic moieties. [v]

One attractive route for electrode immobilization of redox-active species relies on noncovalent interactions between coplanar aromatic groups, such as pyrene, with graphitic electrode surfaces. [vi] This strategy has been employed for reversible oxidation of molecular complexes, and also toward catalytic systems. [vii,viii] Our group has explored covalent attachment of pyrene groups to the polypeptide residues of proteins; upon immobilization of the protein, the assembled cathodes are then competent for bioelectroelectrocatalysis without the use of redox mediators. [ix,x] Similarly, Minteer and co-workers have used pyrene-appended quinones to facilitate electron transfer to immobilized enzymes on carbon nanotube-based electrodes.[xi]

Here we report the preparation and characterization of two new analogues of previously reported catalysts: a rhodium proton-reduction catalyst reported by Kölle and Grätzel[xii], and a rhenium CO_2 reduction catalyst reported by Lehn and co-workers[xiii]. We further characterized their electrochemical and catalytic turnover properties in acetonitrile

Synthesis of Compounds

Synthesis of the pyrene-appended ligand was achieved by coupling 2,2'-dipyridyl-4,4'-carboxylic acid to 1-pyrenylmethylamine in two steps. First the carboxylic acid was converted to the acid chloride using thionyl chloride. Excess thionyl chloride was then removed and the acid chloride was then coupled to 1-pyrenylmethylamine by refluxing in acetonitrile in the presence of a non-nucleophilic base (Scheme 1.1). The resulting compound was a highly insoluble and air stable brown powder.

This compound was fully characterized before being used to synthesize complexes **1** and **2** (Scheme 1.2)**.** Complex **1** was obtained by refluxing $[Cp^*RhCl_2]_2$ with **P** in dichloromethane for 12 hours. The desired product was then isolated by recrystallization, which yielded an air stable yellow solid. Complex **2** was similarly obtained by refluxing

[$Re(CO)_5Cl$] in toluene for 12 hours. The product was then isolated by recrystallization, which yielded an air stable orange solid. These compounds were then characterized by ^{1}H NMR, ^{13}C NMR, and ESI Mass Spectrometry.

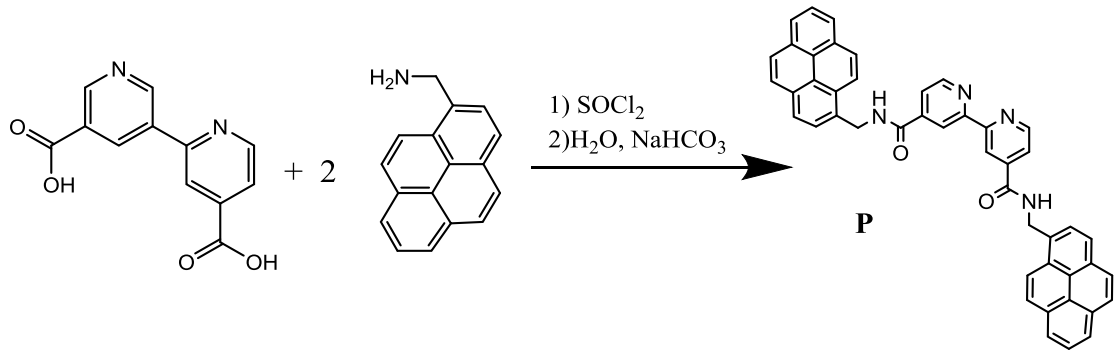

Scheme 1.1 Outline of synthesis used to form the pyrene-append bipyridine ligand **P**.

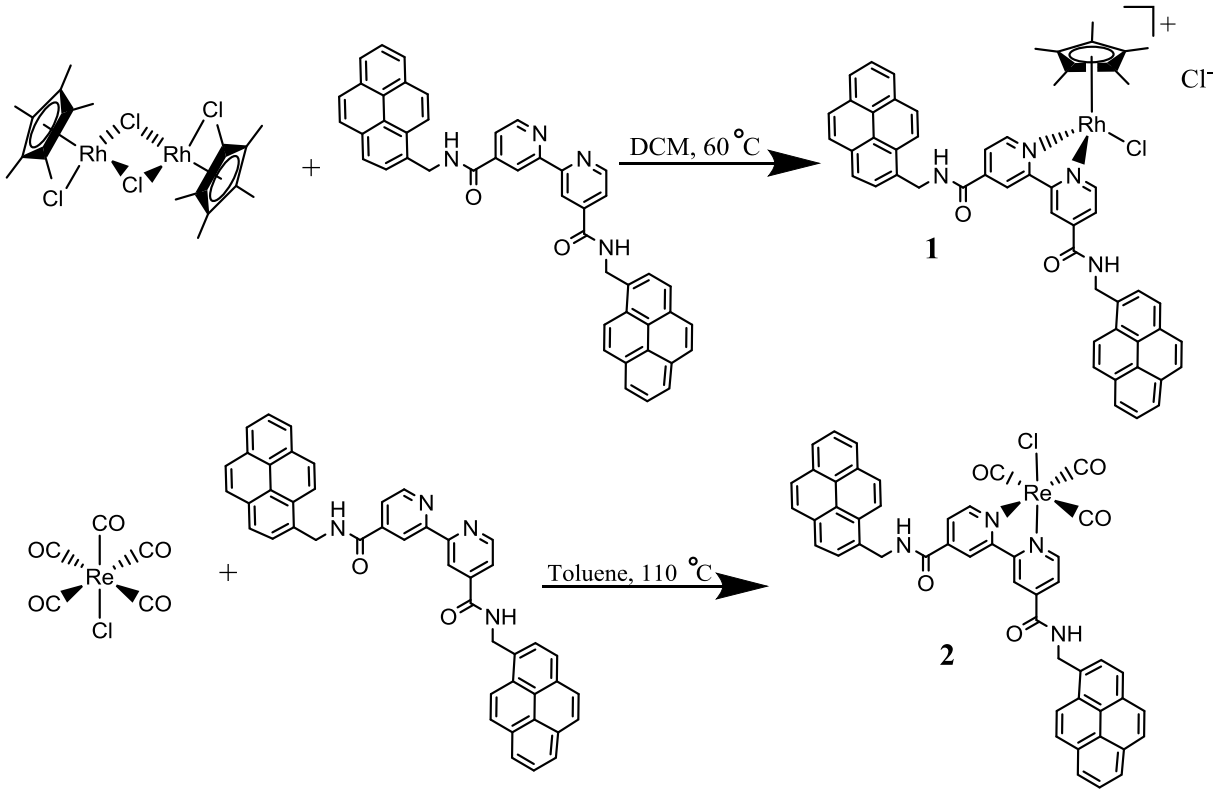

Scheme 1.2 Outline of syntheses used to form pyrene-appended catalysts.

Electrode Preparation

To help facilitate high current densities of the electrode surface, a commercial high surface area carbon black material (Ketjen black, AkzoNobel) was added to a block of highly-oriented pyrolytic graphite (HOPG). Electrodes were prepared using a suspension of Ketjen black in N-methyl-pyrrolidone (containing a small amount of poly(vinylidene fluoride) drop-cast onto the basal plane of highly oriented pyrolytic graphite (HOPG). After heating at 70°C for four hours, the electrodes were ready for use or catalyst immobilization. The complexes were then immobilized on the electrodes by soaking them in a solution of either **1** or **2** for 12 hours. The electrodes were then rinsed with acetonitrile to remove any unbound compounds on the surface.

Electrochemistry of Surface-Attached Complexes

The electrocatalytic properties of the immobilized complexes were tested by running cyclic voltammograms of the electrodes. The voltammetry was carried out with 0.1M NBu_4PF_6 in CH_3CN as the supporting electrolyte, a platinum wire as the counter electrode, and a silver wire immersed in a solution of 0.1 M NBu_4PF_6 as a reference electrode. All reported voltages are versus the ferrocenium/ferrocene redox couple (denoted as $Fc^{+/0}$).

Electrodes with immobilized **1** show a redox feature centered at -1 V (Figure 1.1). The return anodic feature peaks near -0.6 V, and is narrower than the cathodic feature. No other redox features were observed in the electrochemistry. The peak separation of the event is ~400 mV, which decreases as the scan rate decreases, suggesting a charge transfer delay perhaps due to the high surface area carbon material. The peak currents of the cyclic voltammetry was measured at various can rates. The linear relationship between peak current and the scan rate suggests that the species is bound to the surface (Figure 1.2).

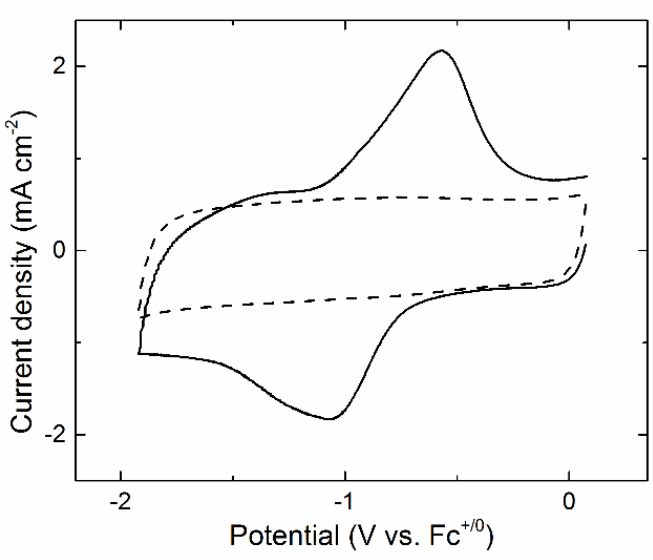

Figure 1.1 Cyclic voltammetry of **1** immobilized on carbon black electrode (solid line) and blank electrode background (dashed line).

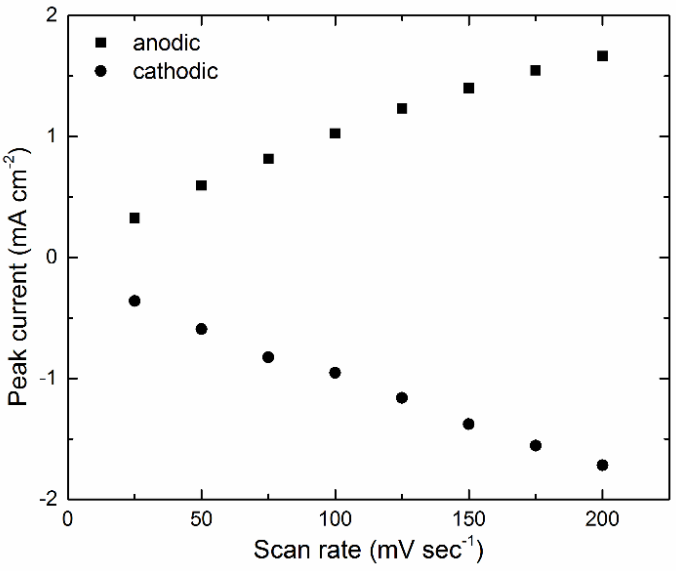

Figure 1.2 Dependence of peak currents (from cyclic voltammetry) for **1** versus scan rate. The linear dependence indicates a non-diffusional surface-bound redox process.

[Cp*Rh(bpy)Cl]Cl undergoes a reversible two-electron reduction near -1 V in MeCN.[xii, ,xiv] Similarly free **1** in solutions undergoes a reversible redox event at -1.25V in dichloromethane (Figure 1.3). While the solvents are not identical, the similarity in redox

potential indicates that **1** displays the same type of electrochemical properties as the one initially reported by Kölle and Grätzel. The reduction potential of -1 V for immobilized **1** is consistent with these values, since the carboxamide substituents of **P** are electron-withdrawing and so the reduction potential will be shifted lower. Reduction of the rhodium complex results in loss of the inner-sphere chloride ligand and formation of a five-coordinate Rh^{I} species. Since the redox process is coupled to loss of chloride, the observed peak separation of greater than 60 mV is also expected.[xv] Assigning our redox event as a two-electron process and using the total charge transferred gives a surface coverage of **1** of 26 nmol cm^{-2}, far higher than coverage expected for a planar electrode, attributable to the carbon black substrate used here.

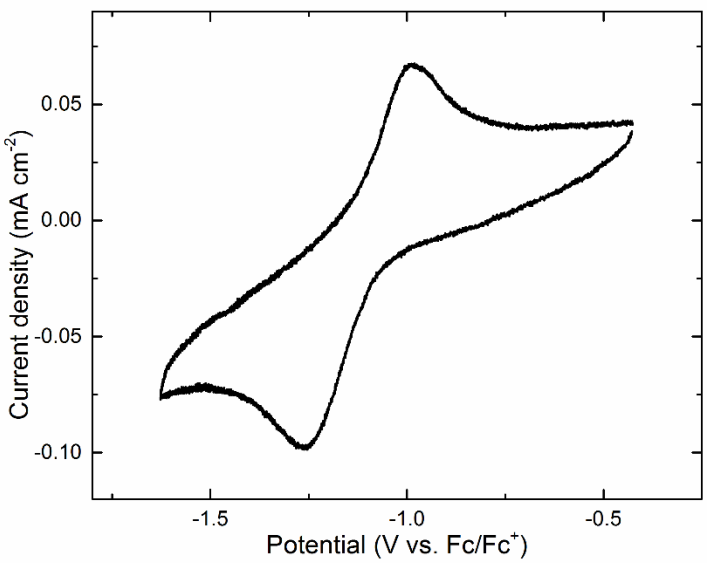

Figure 1.3 Cyclic voltammetry of **1** dissolved in dichloromethane under Ar.

Surface-immobilized **1** is a catalyst for H^{+} reduction. Upon addition of H^{+} to the electrolyte added in the form of tosic acid, cyclic voltammograms display loss of redox reversibility and increased cathodic currents. This becomes more pronounced for further additions of acid (Figure 1.4). Each subsequent addition results in higher catalytic current with background voltammograms only displaying a minor increase in cathodic current. At an acid concentration of 14 mM, the catalytic current plateaus at a steady state current density

slightly above 2 mA cm^{-2}. Using the surface loading data calculated above, this steady state current density corresponds to a turnover frequency of 0.95 sec^{-1}.[xv]

Cyclic voltammograms of immobilized **2** show multiple reduction peaks at -1.34 V, -1.59 V, and -1.84V (Figure 1.5). These peaks compare well against the redox events for **2** in solution (Figure 1.6). By comparing the redox events of the immobilized catalyst, with the free ligand, we can assign each of the redox events to certain electrochemical reactions (Figure 1.7). The free ligand exhibits reductions at -1.21 ($bpy^{0/-}$) and -1.7 V ($pyrene^{0/-}$) with a return oxidation at -1.5 V. For **2,** we can then assign the reduction at -1.34 V to the dipyridyl reduction, the next reduction is the assigned to the pyrene reduction, so the final reduction at -1.84 V is the $Re^{+/0}$, which is the reduction event that drives electrocatalysis. Another oxidation wave is observed at -0.2V. This peak is believed to be the result of the oxidation of a Re-Re dimer that forms due to the reduction of the rhenium center. This reduction leads to a loss of Cl and leaves two five-coordinate metal centers. These can then dimerize to form $[Re(\mathbf{P})(CO)_3Cl]_2$. We believe that the oxidation wave oxidizes this dimer back into the original monomers. Like **1**, the peak currents for **2** are linearly dependent on the scan rate, which is consistent with surface bound complexes (Figure 1.8).

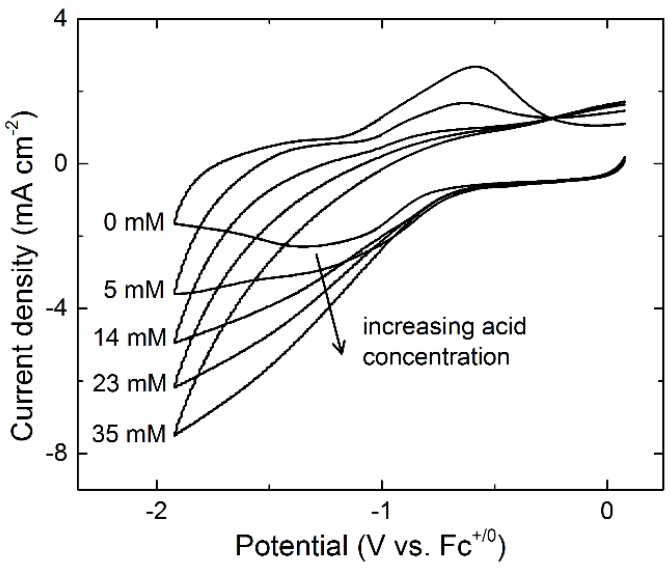

Figure 1.4 Changes in CV response of immobilized **1** in presence of increasing concentrations of *p*-toluenesulfonic acid. Onset of catalytic response occurs near -0.75 V.

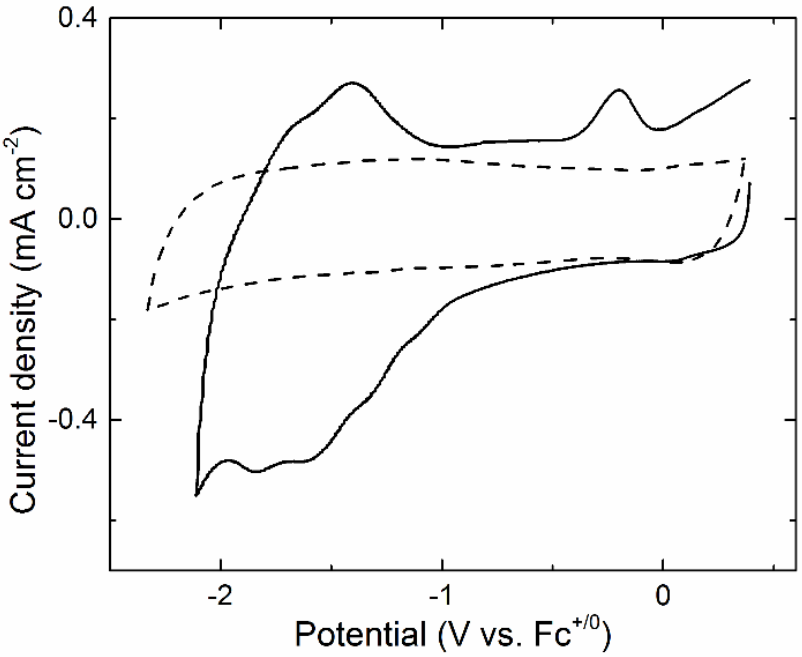

Figure 1.5 Electrochemistry of **2** immobilized on carbon black electrode (solid line) and blank electrode (dashed line).

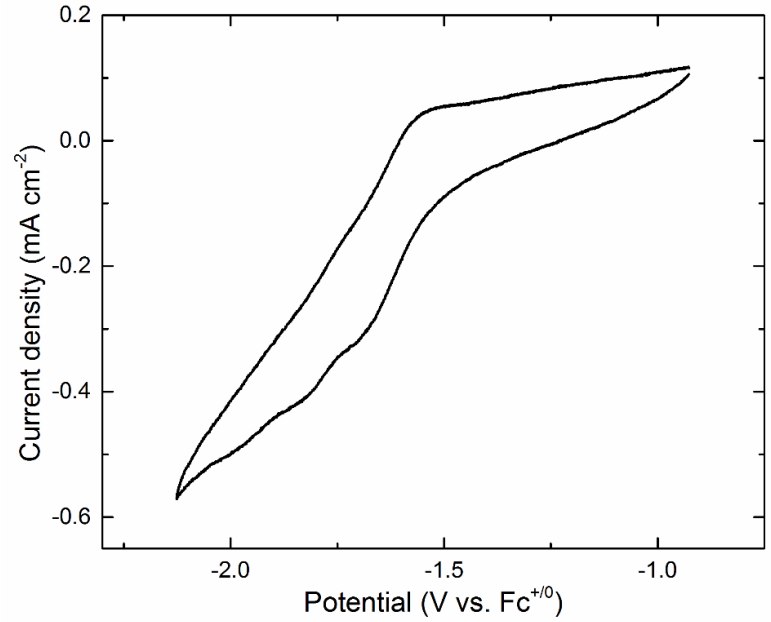

Figure 1.6 Cyclic voltammetry of **2** dissolved in dichloromethane containing 0.1 M tetrabutylammonium hexafluorophosphate at 200 mV/s.

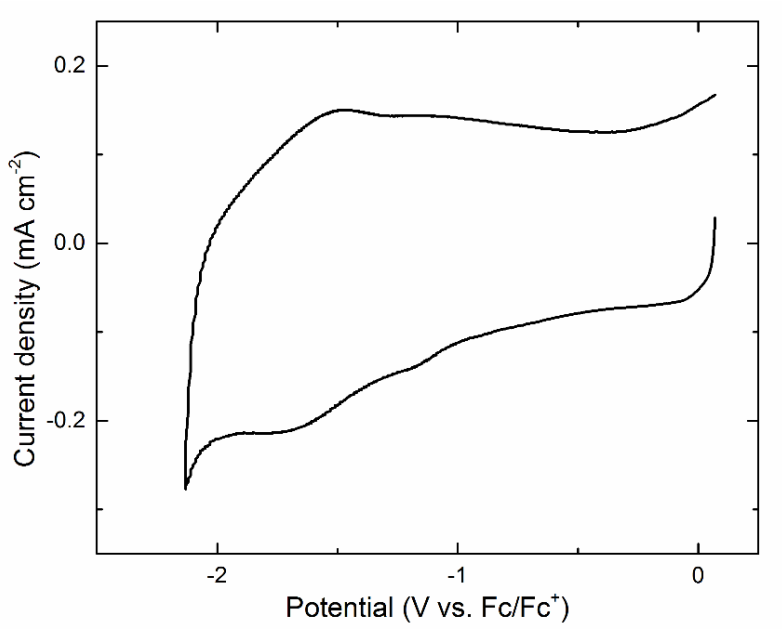

Figure 1.7 Cyclic voltammograms of immobilized **P**. The compound was immobilized by soaking the electrode in a DMSO solution of **P** for 12 hours.

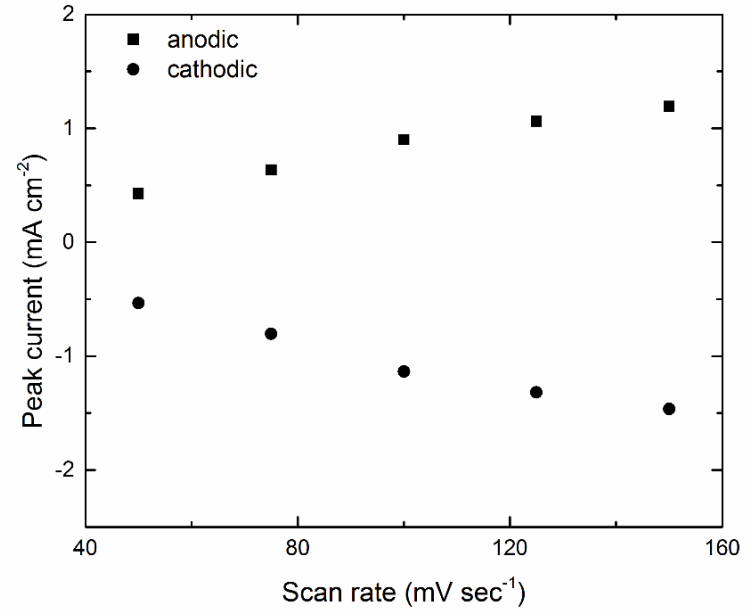

Figure 1.8 Dependence of peak currents (from cyclic voltammetry) for **2** versus scan rate. The linear dependence indicates a non-diffusional surface-bound redox process.

Surface-immobilized 2 is a catalyst for CO_2 reduction to CO. By comparing the cyclic voltammetry of an electrode with immobilized 2 both under argon and under carbon dioxide, we can see that there voltammograms are very similar until the final reduction at -1.8 V, which confirms our assignment of the rhenium reduction peak and the catalytic ability of 2 (Figure 1.9). The catalytic wave at this potential has a ratio of catalytic current to peak current (i_{cat}/i_p) of 3.6, similar to the enhancement observed for $Re(bpy)(CO)_3Cl$ in solution, but lower than the 18.4 enhancement observed for a solution soluble di-tert-butyl-bipyridine analog.[xvi] Background scans further confirm that in the absence of either CO_2 or 2 there is no catalytic current.

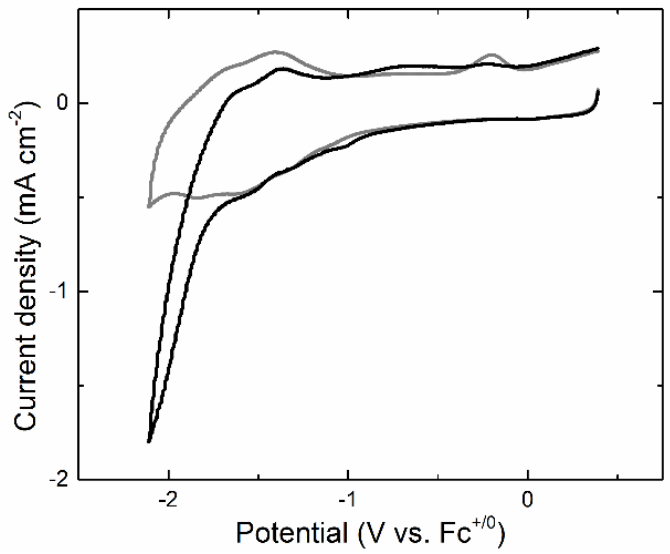

Figure 1.9 Cyclic voltammetry of immobilized **2** under Ar (gray line) and under CO_2 (black line).

X-Ray Photoelectron Spectroscopy of Immobilized Complexes

The electrodes were interrogated by x-ray photoelectron (XP) spectroscopy. This allows the study of the various elements bound to the graphitic surface. Before immobilization of our metal complexes, the surfaces show only peaks for carbon (C 1s), nitrogen (N 1s), fluorine (F 1s), and a small contribution from oxygen (O 1s). Following preparation with **1**, new peaks appear that are consistent with rhodium(III) , chloride (Cl 2s; Cl 2p), and an increased nitrogen (N 1s) (Figure 1.10). XP spectra of the N 1s and Rh 3d peaks under

acidic conditions and after electrocatalytic turnover are also shown (Figure 1.11). These show the presence of only one type of Rh species on the surface. There are also no new peaks growing in after catalytic turnover, which indicates that the complex on the surface is likely the same as the original complex initially attached. Analysis of the Cl peak in the spectra show a loss of Cl after cyclic voltammetry (Figure 1.12). This backs up the claim that Cl is lost upon reduction of the Rh. The Cl from the initial complex was then likely substituted by a solvent molecule and was subsequently washed away during preparation for XPS. XP spectra collected for electrodes soaked in solutions of an analogous complex not appended with pyrene ([Cp*Rh(1,10-phenanthroline)Cl]Cl) do not show analogous peaks (Figure 1.13) indicating that pyrene is necessary for surface attachment.

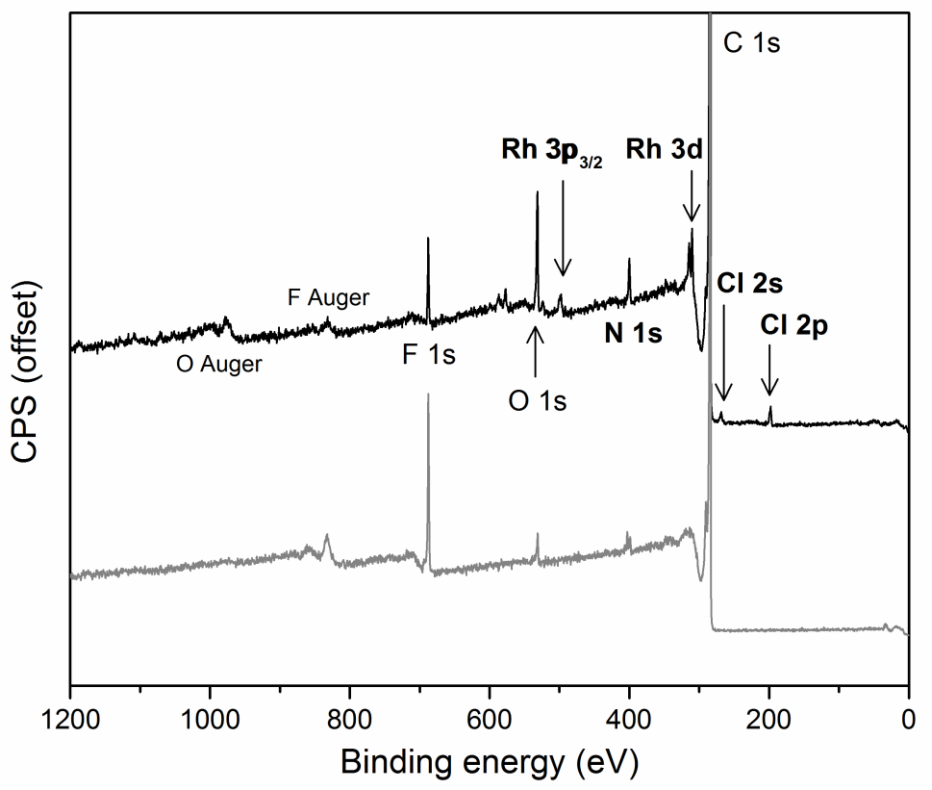

Figure 1.10 XP survey spectra for blank carbon electrode (gray line) and **1** immobilized on carbon electrode (black line).

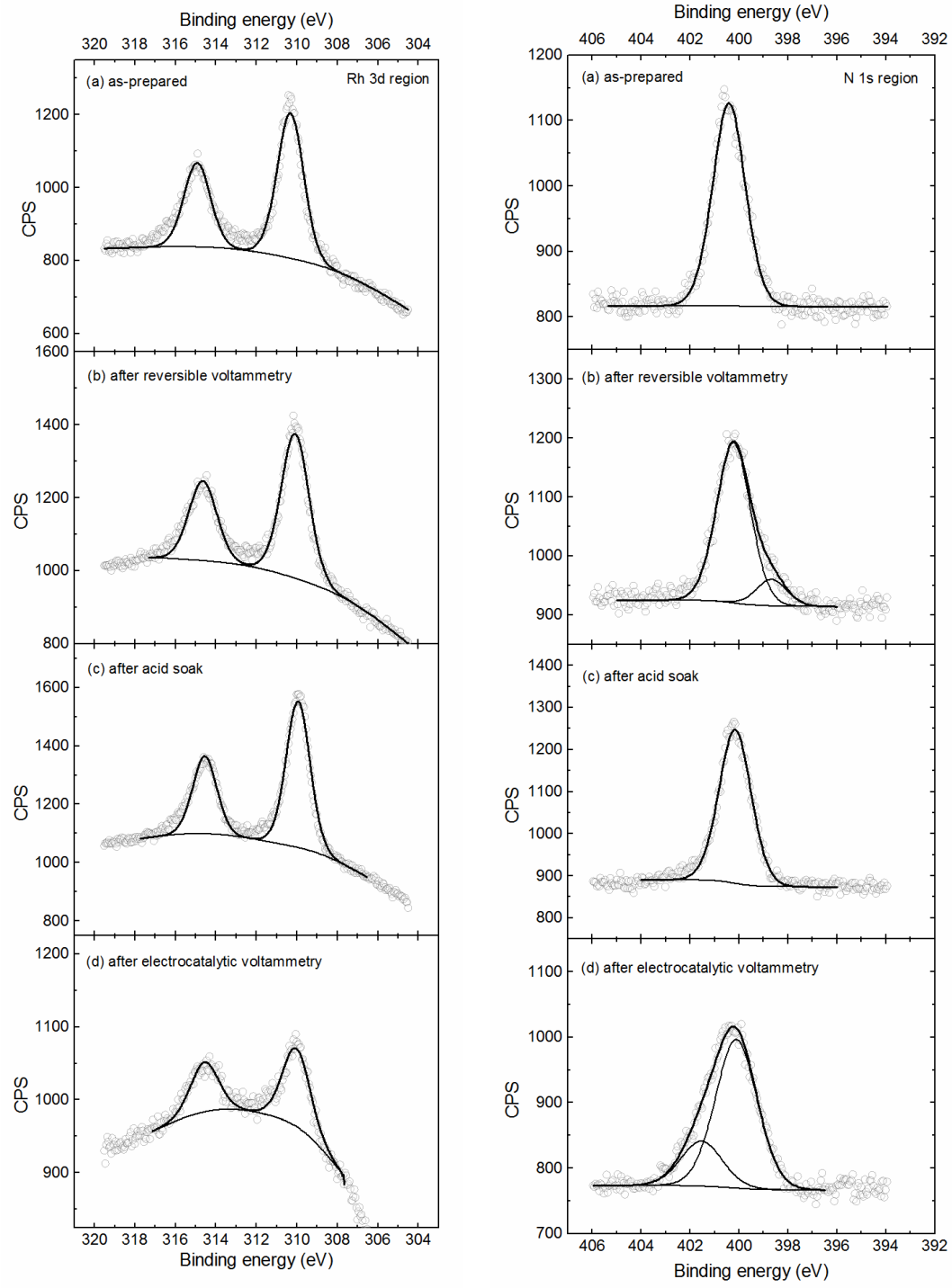

Figure 1.11 Rh 3d XP spectra (left) and N 1s for **1** immobilized on carbon electrode. (a) Electrode as-prepared; (b) after reversible cyclic voltammetry; (c) after soaking in tosic acid for 1 hr; (d) after catalytic voltammetry.

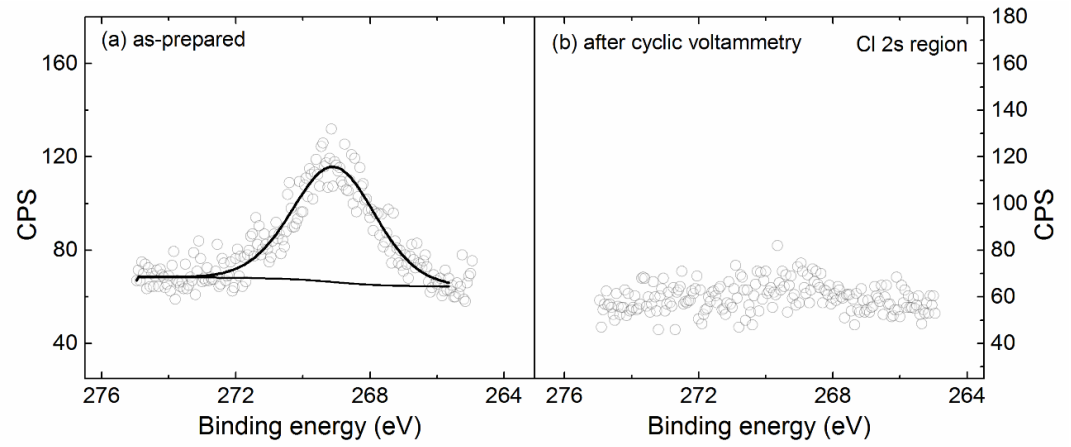

Figure 1.12 Cl 2s XP spectra for **1** immobilized on carbon electrode. (a) Electrode as-prepared; (b) after reversible cyclic voltammetry.

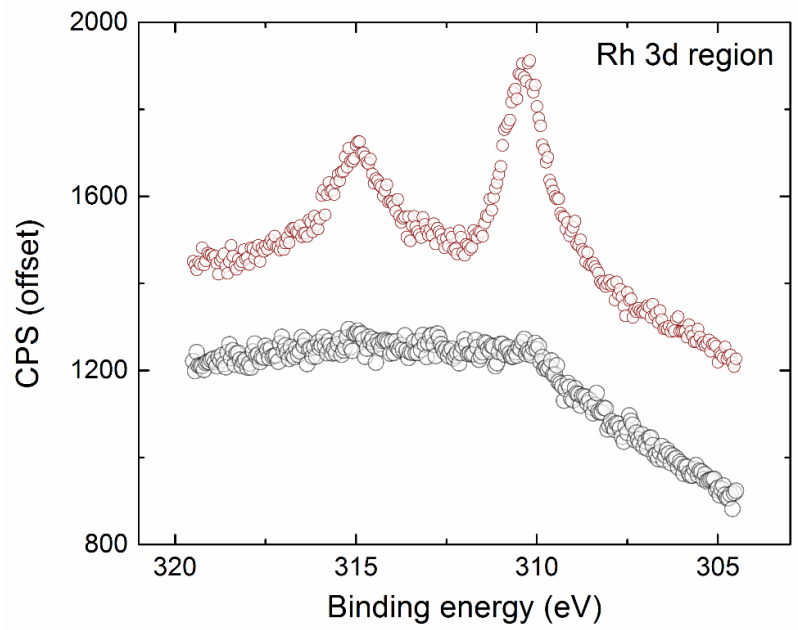

Figure 1.13 Comparison of Rh 3d XP spectra for carbon electrodes soaked in **1** (red) or ([Cp*Rh(1,10-phenanthroline)Cl]Cl] (gray) followed by soaking in acetonitrile.

Similarly, electrodes soaked in solutions containing **2** show new XP peaks corresponding to rhenium(I) (Re 4f, 4d), chloride (Cl 2s, 2p), and increased nitrogen (N 1s)

(Figure 1.14). XP spectra of the Re 4d and Re 4f peaks under acidic conditions and after electrocatalytic turnover are also shown (Figure 1.15). These show the presence of only one type of Re species on the surface. There are also no new peaks growing in after catalytic turnover, which indicates that the complex on the surface is likely the same as the original complex initially attached. Analysis of the Cl peak in the spectra show a loss of Cl after cyclic voltammetry. This backs up the claim that Cl is lost upon reduction of the Rh. The Cl from the initial complex was then likely substituted by a solvent molecule and was subsequently washed away during preparation for XPS. Electrodes soaked in solutions of [Re(2,2'-dipyridyl)$(CO)_3$Cl] show no signal for Re 4f. Thus, pyrene binding is responsible for the association between our complexes and the electrode surface.

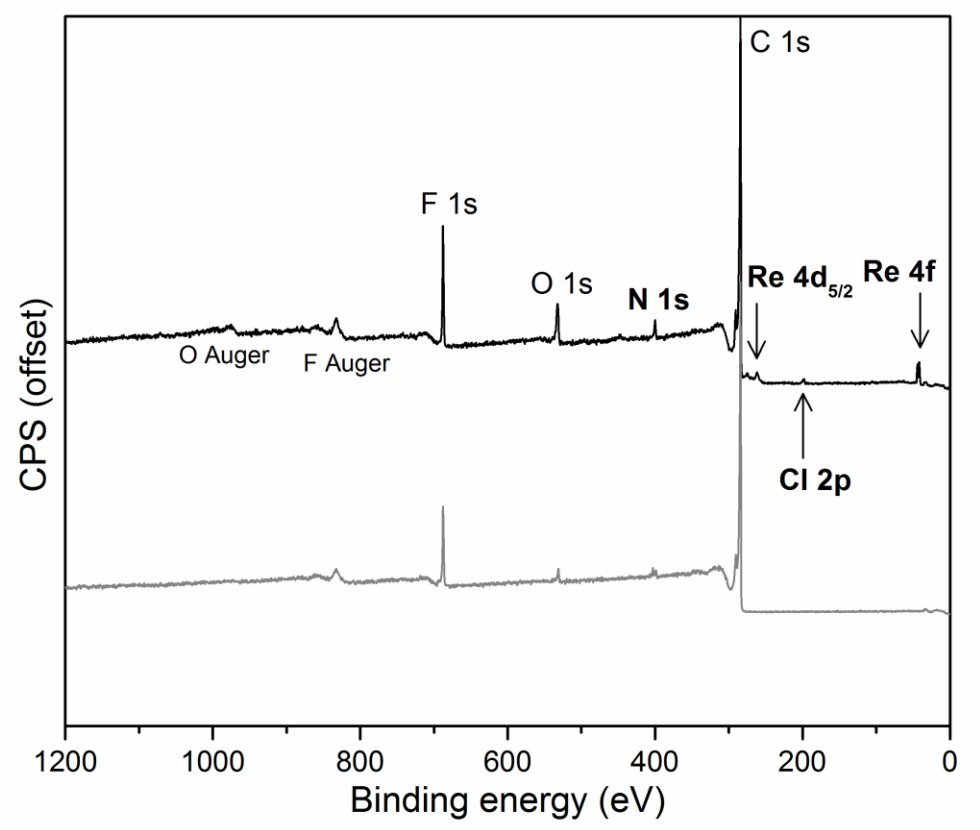

Figure 1.14 XP survey spectra for blank carbon electrode (gray line) and **2** immobilized on carbon electrode (black line).

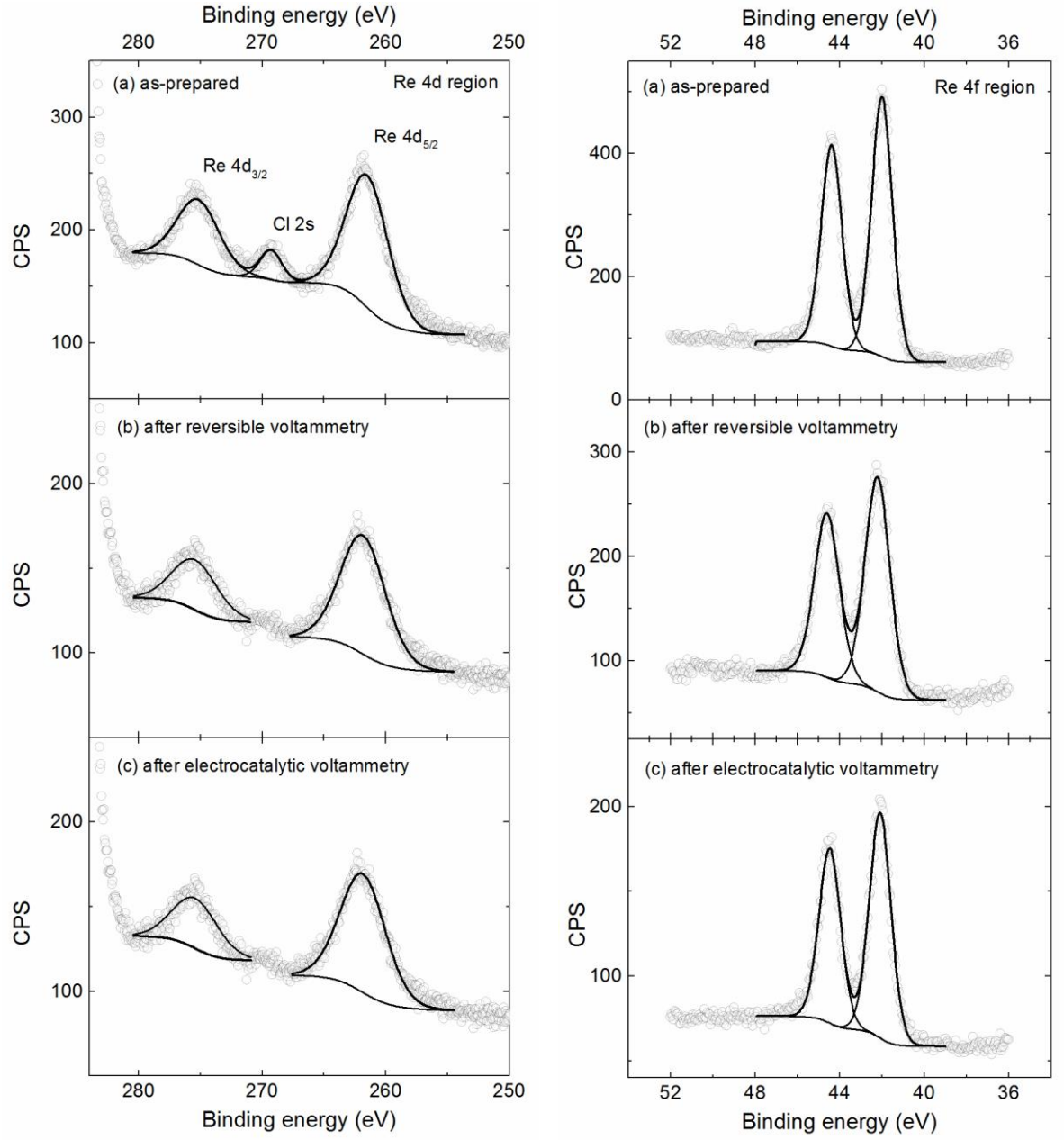

Figure 1.15 Re 4f XP (left) and Re 4d and Cl 2s (right) spectra for **2** immobilized on carbon electrode. (a) Electrode as-prepared; (b) after reversible cyclic voltammetry; (c) after electrocatalytic voltammetry.

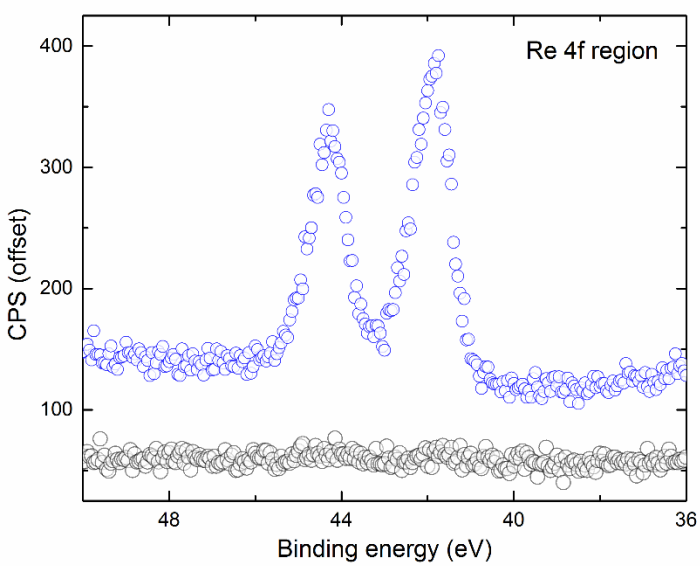

Figure 1.16 Comparison of Re 4f XP spectra for carbon electrodes soaked in **2** (blue circles) and [Re(2,2'-dipyridyl)$(CO)_3Cl$] (gray circles) followed by soaking in acetonitrile to remove complexes not strongly bound.

Bulk Electrolysis

H_2 production was confirmed by gas chromatograph (GC) of headspace in a closed two-compartment cell during a controlled potential electrolysis of the immobilized catalyst with 5 mM *p*-toluenesulfonic acid. A voltage of -1.1 V was maintained for 1.25 hours over which a sufficient net charge was passed through to generate 0.86 mL of H_2 (Figure 1.17). We found that 0.90 mL of H_2 was produced (from GC), which confirms a quantitative H^+ reduction within a 10% error range. This experiment demonstrates the remarkable stability of the immobilization strategy of the compound, where over 1.25 hours the catalytic current remains above background levels, although the current did decrease by 30% per hour, indicative of catalyst deactivation or loss from the surface.

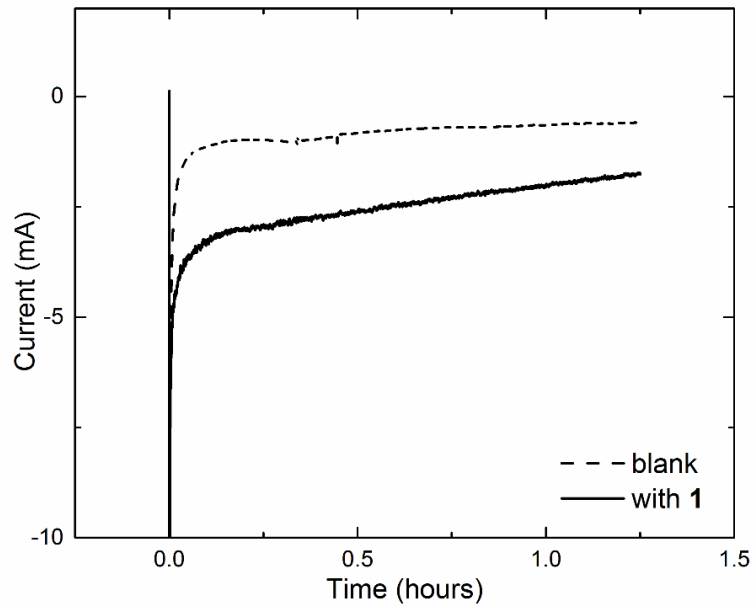

Figure 1.17 Steady state current densities during the controlled-potential electrolysis of a blank carbon electrode (dashed line) and an electrode prepared with **1** (solid line).

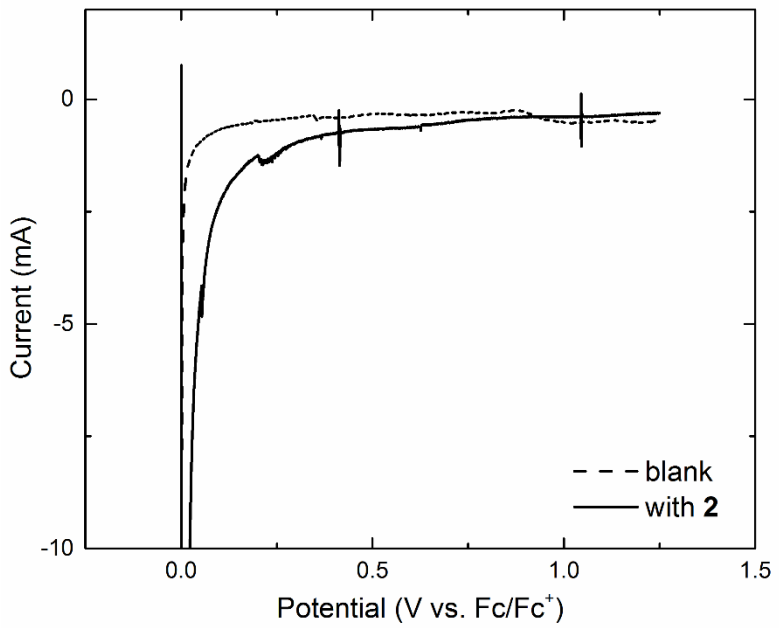

Figure 1.18 Steady state current densities during the controlled-potential electrolysis of a blank carbon electrode (dashed line) and an electrode prepared with **2** (solid line) under an atmosphere of CO_2.

The gas chromatograph analysis of headspace gas in a CO_2-purged cell with an electrode soaked with 2 following a 1.25 hour electrolysis at -2.3 V confirms production of CO (Figure 1.18). By charge transfer, we assume 0.39 mL of CO would be produced, of which we found 0.25 mL of CO. This corresponds to a Faradaic efficiency of nearly 80% and a TON of 58. No H_2 was produced with immobilized **2**, but a small amount was found in control experiments without **2**. The electrodes soaked with 2 are not as robust as electrodes soaked with 1 as shown in the bulk electrolysis, where 2 reached background levels of current within an hour whereas 1 did not. The significant current drop off may be attributable to formation of catalytically inactive rhenium-rhenium dimers instead of reacting with CO_2. Another possible explanation for this behavior could be reduction of the pyrenyl moieties at the very negative potentials required for operation of the catalyst; reduction of pyrene could result in Coulombic repulsion with the surface, or loss of planarity and binding.

Conclusion

These results show that immobilization of molecular catalysts via pyrene groups is a promising general strategy for studying electrocatalysis of fuel-forming reactions and demonstrates a noncovalent surface attachment of a molecular CO_2 reduction catalyst. Encouragingly, despite the extreme potentials required for CO_2 reduction, these electrodes are sufficiently stable for future detailed studies as indicated by the length of active catalysis demonstrated by the rhodium complex. Such comparisons will help in the optimization of functional assemblies for solar-fuel production.

Chapter II

Further Study of Pyrene-Appended Ligand Applicability in a Manganese, Ruthenium and Iridium Complexes

Introduction

Few studies of the electrochemistry of noncovalently immobilized redox couples are currently available, and even fewer have examined redox potentials more negative than –1 V. The previous work focused on noncovalent immobilization of molecular catalysts for fuel-forming reactions. Deronzier et al. have functionalized an electrode with a [Cp*Ir] system via a polymerization route. [xvii] A number of pyrene-appended polypyridyl complexes of ruthenium have been synthesized, [xviii] but none have yet been examined at negative potentials upon noncovalent immobilization on carbon electrode surfaces. [xix, xx, xxi] Negative potentials are required for most fuel-forming catalytic processes, and thus developing an understanding of the activity and stability of noncovalently immobilized compounds under reductive conditions is of particular interest.

Along this line, three new compounds for electrochemical studies at negative potentials are shown here: [Ru(P)(4,4'-dimethyl-2,2'-bipyridine)$_2$]Cl$_2$, [Cp*Ir (**P**)Cl]Cl, and Mn(**P**)(CO)$_3$Cl. X-ray photoelectron spectroscopy confirmed successful immobilization of these complexes on high surface area carbon electrodes, with the expected elemental ratios and oxidation states for the desired compounds. Electrochemical data revealed a reversible reduction of the ruthenium complex near –1.4 V, and reduction of the iridium complex near –0.75 V. The ruthenium complex showed good stability, with reversible currents operative beyond one hour, while the iridium complex showed complex electrochemistry suggestive of ligand exchange to form multiple complexes on the surface. The manganese complex displayed showed good stability as well with observable redox events occurring beyond an hour of continuous reductive cycling. The catalytic ability of this compound was also characterized, but product detection still needs to be done to confirm catalysis.

Synthesis of Compounds

Pyrene-appended complex **3** was synthesized by refluxing $[Ru(Cl)_2(4,4'\text{-dimethyl-}2,2'\text{-bipyridine})_2]Cl_2$ with **P** in dimethylformamide for 24 hours. The product was then purified through a series of recrystallizations with methanol, dichloromethane and diethyl ether yielding an air stable red solid. Similarly, **4** was synthesized by treating refluxing **P** with 0.5 equivalents of $[Cp^*IrCl_2]_2$ in acetonitrile for 12 hours. The product was then recrystallized in dichloromethane yielding an air stable yellow solid. Complex **5** was synthesized by refluxing $[Mn(CO)_5Br]$ with **P** for 16 hours in dichloromethane. The product was then recrystallized in hexane yielding a light-sensitive orange solid (Scheme 2.1).

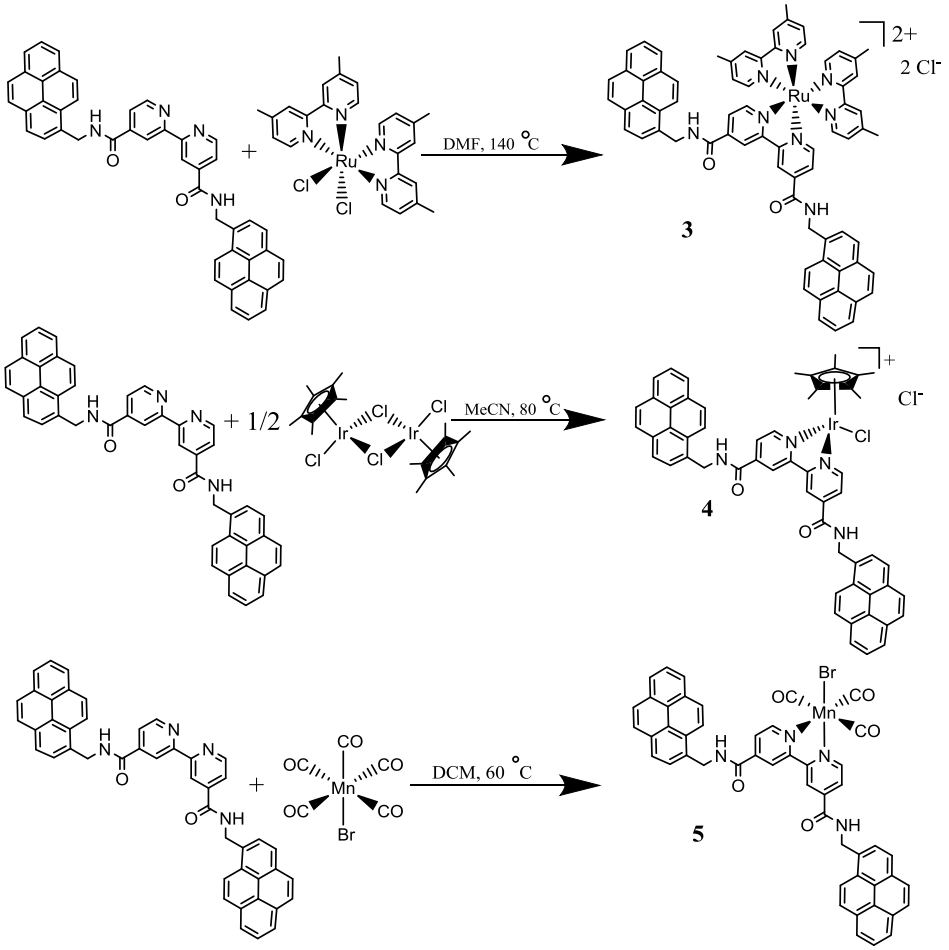

Scheme 2.1 Outline of the syntheses used to form three different compounds suitable for surface-attachment using **P**.

Electrochemistry of Surface-Attached Compounds

Like in the previous study, functionalization of high surface area Ketjen black electrodes with **3, 4**, or **5** was accomplished by soaking the electrodes in a dilute solution of the respective compounds for 12 hours. This allowed for high surface loading of immobilized metal complex to carry out the electrochemical work. [xxii] After soaking the Ketjen black electrodes, the functionalized electrodes were rinsed with clean acetonitrile to remove loosely associated complexes.

Cyclic voltammograms collected with electrodes featuring immobilized **3** displayed a feature centered at –1.64 V and a cathodic feature at –1.75 V (Figure 2.1). The return anodic current peaked at –1.5 V, and no additional oxidation features were found up to –0.3 V. This reversible redox event corresponds to a bipyridine ligand-centered reduction of immobilized **3**, as reported by previous studies of **3** and its derivatives. [xxiii] Notably, only a single reduction process was observable, in contrast to the multiple ligand-centered reductions typically observable for [Ru(2,2'-bipyridine)$_3$]Cl$_2$.

The peak-to-peak separation was ~250 mV at a scan rate of 50 mV/s. This splitting decreases with decreasing scan rate likely due to improved response time for the electrode. Inspection of scan-rate dependent data for the peak currents showed a linear correlation between peak currents and the scan rate, consistent with a surface-immobilized process. Similar redox behavior was observed for **1** dissolved in solution, with a quasireversible reduction feature centered at –1.55 V, with the cathodic current peak at –1.51 V and the anodic current peak at –1.59 V. The peak-to-peak separation was only ~100mV, smaller than that of the immobilized complex. A square root dependence of the peak currents on the scan rate confirmed the redox couple was freely diffusing in solution. The similarity of the peak position and reversibility suggests that the complex retains similar electrochemical properties upon immobilization, as expected for the mild immobilization route used here. However, the midpoint potential ($E_{1/2}$ value) for immobilized **1** was shifted by nearly 100 mV versus freely diffusing analogue **3**. This suggests that the methyl groups on the 4,4′-dimethyl-2,2′-bipyridyl ligands result in a more electron-rich metal complex in the case of

1 compared to **3**, despite the electron-withdrawing carboxamide substituents on our pyrene-appended ligand **P**.

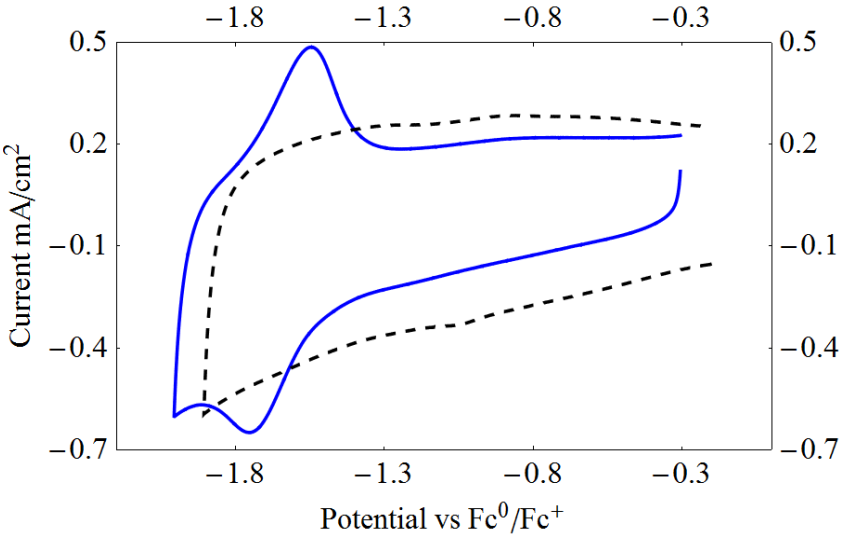

Figure 2.1 Electrochemistry of **3** immobilized on carbon black electrode (solid line) and blank electrode (dashed line).

A stability test of immobilized **3** was carried out by cycling an electrode with **3** 120 times from –0.9 V to –1.9 V at 50 mV/s (Figure 2.2). The area under the anodic peak was then integrated and plotted against the total time elapsed to measure the approximate coverage of the metal complex on the surface. The initial coverage was about 9 nanomol cm^{-2}, a similar to those we have encountered for other pyrene-immobilized complexes. The surface coverage decreased steadily until the 100th scan, at which point the coverage stabilized at ca. 2 nanomol cm^{-2}. This loss of **1** corresponds to an 81% loss of the electroactive compound. Because of the low loading of **1** and the relatively large solution volume (7.5 mL), loss of material from the surface would result in the virtually complete loss of the electrochemical signal.

A separate stability test was conducted by cycling an electrode featuring **3** every 10 minutes to determine if the complex is stably immobilized during simple immersion in electrolyte solution (Figure 2.2). Here, the observed redox process is lost at a much slower rate, as only 27% was lost from the surface after three hours. This difference strongly

suggests that formation of the reduced form of the compound resulted in acceleration of loss of the reversible reduction. XP spectra collected following electrochemical cycling in both cases confirmed some Ru remaining on the surface; however, all signals were attenuated confirming loss of **3** from the surface.

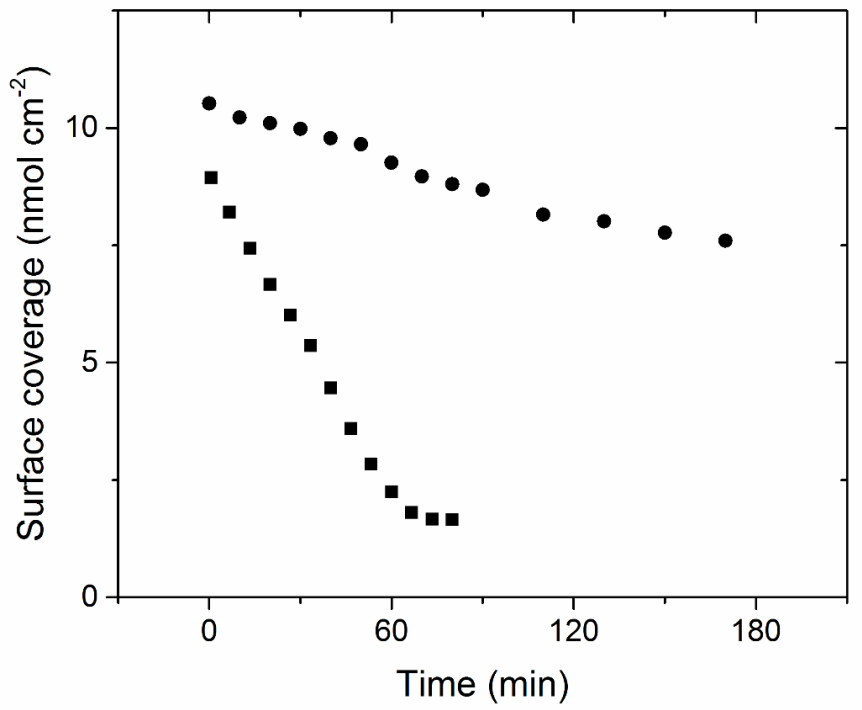

Figure 2.2 Surface coverage of **3** as a function of time in minutes. Filled circles: potential cycling every 10 minutes; filled squares: continuous potential cycling.

The cyclic voltammogram of immobilized **4** showed a reduction process peaking at –1.2 V and two distinct anodic processes peaking near –0.9 V and –0.5 V on the first cycle (Figure 19). On a second cycle of voltammetry, a new cathodic process appears at –0.8 V. The reductive process remained apparent at –1.2 V, but was diminished upon the second cycle. In the solution-phase electrochemistry of the analogous complex of 2,2´-bipyridyl, the more positive reduction event was attributed to the reduction of the acetonitrile adduct and the more negative process was attributed to the chloride adduct. [xxiv] This acetonitrile complex forms during the first reductive cycle, which is coupled to loss of chloride from the complex. [xxv] Thus, on the first cycle, reduction of the chloride-bound

[Cp*Ir] complex is observed. For the case of **4**, we postulate that the two observed reduction processes correspond to the acetonitrile- and chloride-bound complexes. Notably, this interpretation of the electrochemical data suggests that both species are present on the surface, suggesting slow ligand exchange at some sites on the high surface area carbon electrode (Figure 2.3).

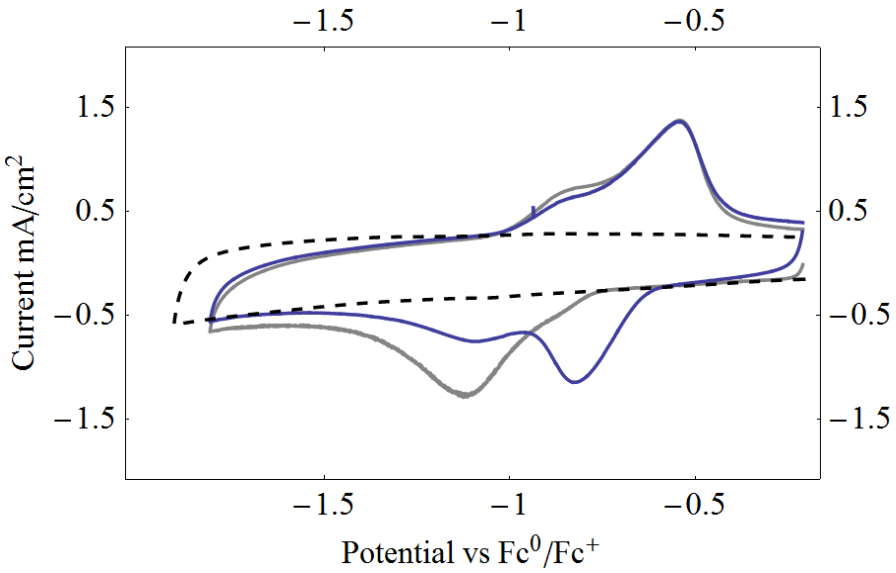

Figure 2.3 Cyclic voltammetry of immobilized **4** under Ar for the first scan (gray), second scan (blue), and blank (black).

Studies of the catalytic ability of surface-attached **5** were conducted next (Figure 2.4). Little change is observed when adding .4mM trifluoroethanol. Due to some interconversion to the solvent adduct species, we see the growth of a new peak at -1V. We also see what could be attributed as catalytic enhancement at -1.5V. The amount of enhancement is so little that it is likely due to proton reduction occurring on the graphitic electrode itself and not because of the iridium catalyst. Upon bubbling of CO_2 in the cyclic voltammetry changes once again. We see the peak at -1V disappear and the onset of catalytic current at -1.2V. Unlike the acidic conditions. We see much greater enhancement of current and the characteristic diminishment of one of the redox peaks. This indicates that some sort of catalytic reaction is occurring. Unfortunately, this type of catalysis is very

unstable. Upon conducting another scan of the same electrode, we see a massive loss of current and the redox event at -.8V (Figure 2.5). This is likely due to desorption of the complex due to conformation change. Due to this instability, no product detection was able to be conducted for the surface-attached complex.

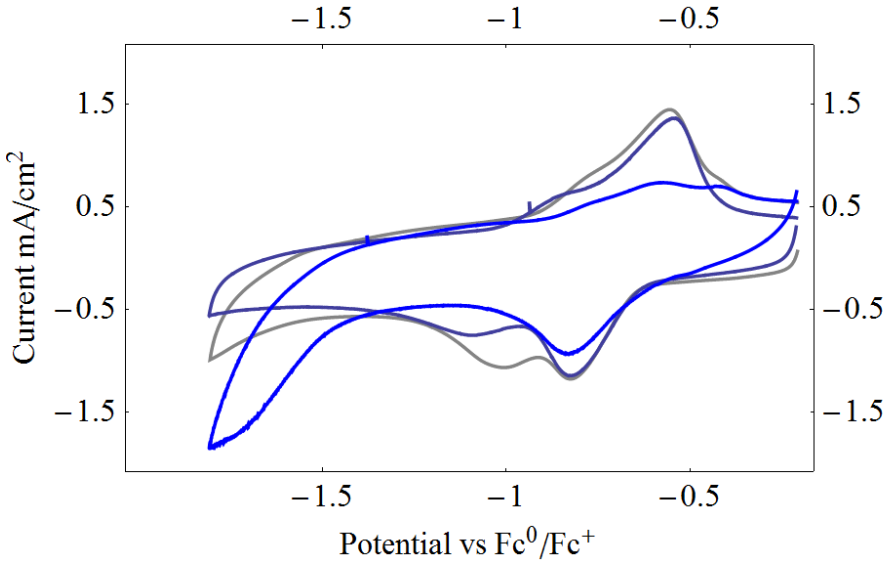

Figure 2.4 Cyclic voltammetry of immobilized **4** under Ar (black), with .4mM trrifluoroethanol (gray), and ,4mM TFE under CO_2 (blue).

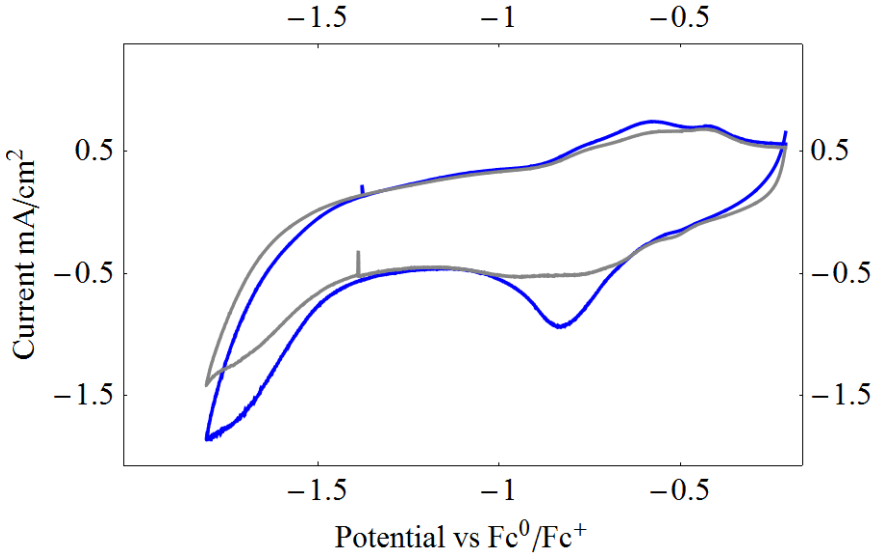

Figure 2.5 Cyclic voltammetry of immobilized **4** under with 4mM TFE under CO_2 for the first scan (blue) and the second scan (gray).

Cyclic voltammograms of immobilized **5** show reduction peaks at -1.4 V, and -1.7V and oxidation waves at 1.4V(broad) and -0.5V (Figure 2.6). These peaks compare well against the redox events for **2** and the free ligand (Figure 1.5 and 1.7). By comparing the redox events of the immobilized catalyst, with the free ligand, we can assign each of the redox events to certain electrochemical reactions (Figure 1.7). The free ligand exhibits reductions at -1.21 ($bpy^{0/-}$) and -1.7 V ($pyrene^{0/-}$) with a return oxidation at -1.5 V. We do not observe the dipyridyl reaction at -1.21V but instead at -1.4V. A similar potential is observed for dipyridyl reduction in **2**. The next reduction at -1.7 is the assigned to the pyrene reduction. We do not observe any further reduction events, so we believe the $Mn^{+/0}$ also occurs very near -1.7V. This is reasonable as the reduction of **2** occurs very near the same voltage. Another oxidation wave is observed at -0.5V. This peak is believed to be the result of the oxidation of a Mn-Mn dimer that forms due to the reduction of the manganese center.

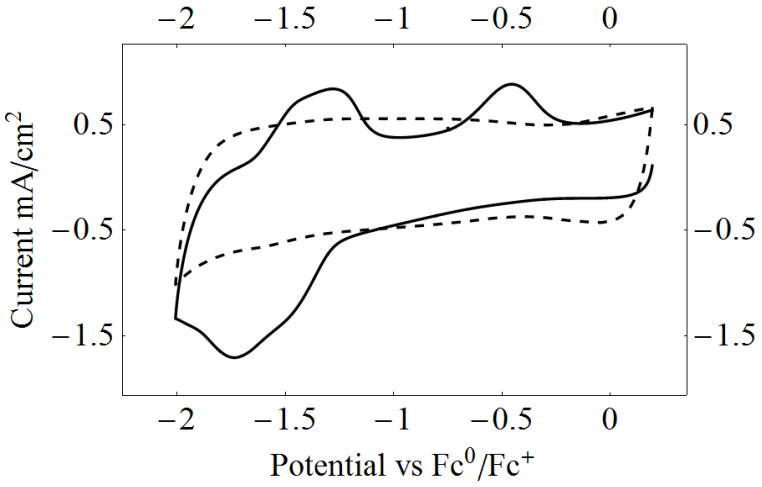

Figure 2.6 Cyclic voltammetry of immobilized **5** under Ar (black) and blank (dashed).

Once again this redox behavior mimics the one found in the previously studied rhenium system. The manganese reduction leads to a loss of Br and leaves two five-coordinate metal centers. These can then dimerize to form $[Mn(\mathbf{P})(CO)_3Br]_2$. We believe that

the oxidation wave oxidizes this dimer back into the original monomers. The electrochemistry of this system closely mirrors that of [$Re(CO)_3$(2,2'-bipyridine)Br] in solution (Figure 2.7). The redox events occur at nearly identical voltages. The major difference being the large amount of broadening found in the surface-attached complex and the slightly more negative potential for the dipyridyl based reduction.

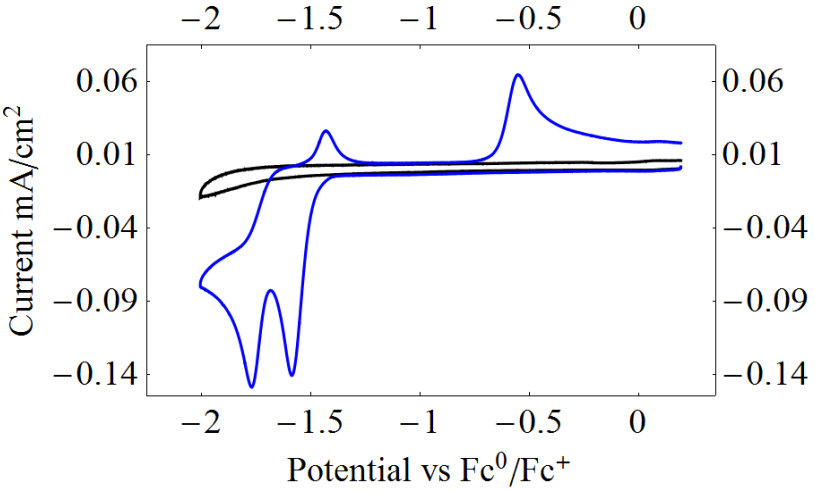

Figure 2.7 Cyclic voltammetry of [$Re(CO)_3$(2,2'-bipyridine)Br] under Ar (blue) and blank (black).

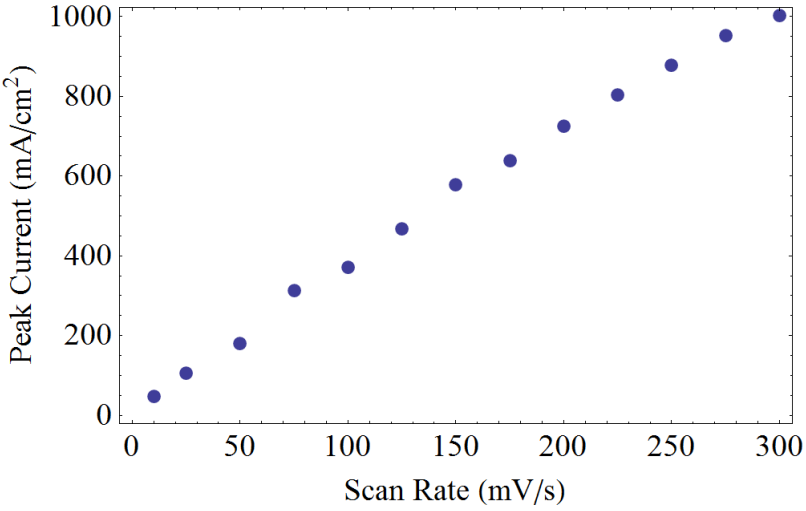

Figure 2.8 Dependence of peak currents (from cyclic voltammetry) for 5 versus scan rate. The linear dependence indicates a non-diffusional surface-bound redox process.

The peak currents for 5 are linearly dependent on the scan rate, which is consistent with surface bound complexes (Figure 2.8). A stability test of immobilized **5** was carried out by cycling an electrode with **5** 160 times from 0.2 V to –2.0 V at 50 mV/s (Figure 2.9). The area under the anodic peak was then integrated and plotted against the total time elapsed to measure the approximate coverage of the metal complex on the surface. The initial coverage was about 54 nanomol cm^{-2}. This amount of loading is five times greater than previous pyrene-immobilized complexes. The surface coverage decreased steadily until the 50^{th} scan, at which point the coverage stabilized at ca. 15 nanomol cm^{-2}. This loss of **5** corresponds to an 72% loss of the electroactive compound, which is also similar to previously studied compounds (Figure 2.9). Because of the low loading of **5** and the relatively large solution volume (7.5 mL), loss of material from the surface would result in the virtually complete loss of the electrochemical signal.

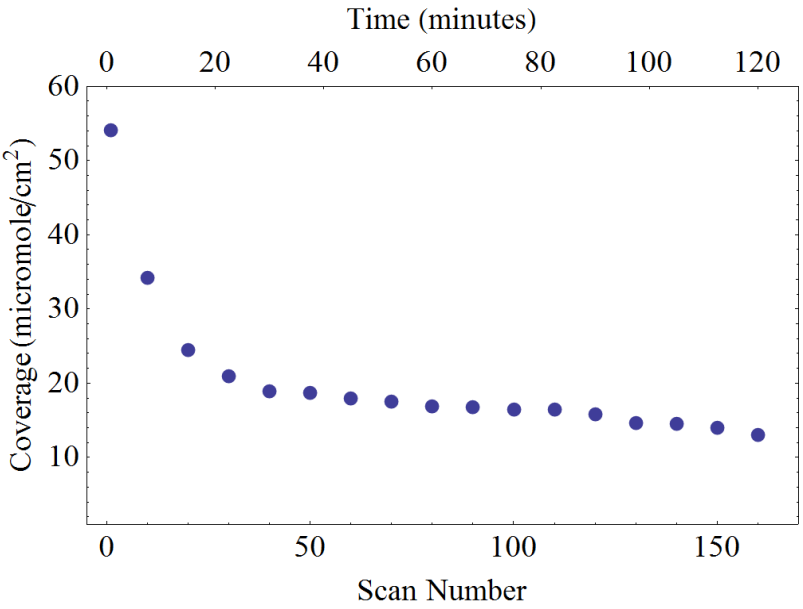

Figure 2.9 Stability test of **5** under continuous cyclic voltammetry cycling.

We believe surface-immobilized **5** is a catalyst for CO_2 reduction to CO. By comparing the cyclic voltammetry of an electrode with immobilized **5** both under argon and under carbon dioxide, we can see that there voltammograms are very similar until the final

reduction at -1.7 V (Figure 2.10). This confirms our assignment of the manganese reduction peak which is being obscured by the pyrene reduction peak. We also see no evidence of catalytic proton reduction by the surface-attached catalyst. Very little if any catalytic enhancement is observed and is likely due to direct proton reduction by the graphitic substrate. Background scans further confirm that in the absence of either CO_2 or **5** there is no catalytic current. To confirm catalysis, product detection must be done. A preliminary test has been conducted that indicated the presence of CO, but due to some experimental error, the bulk electrolysis will be redone to provide definitive proof of catalysis.

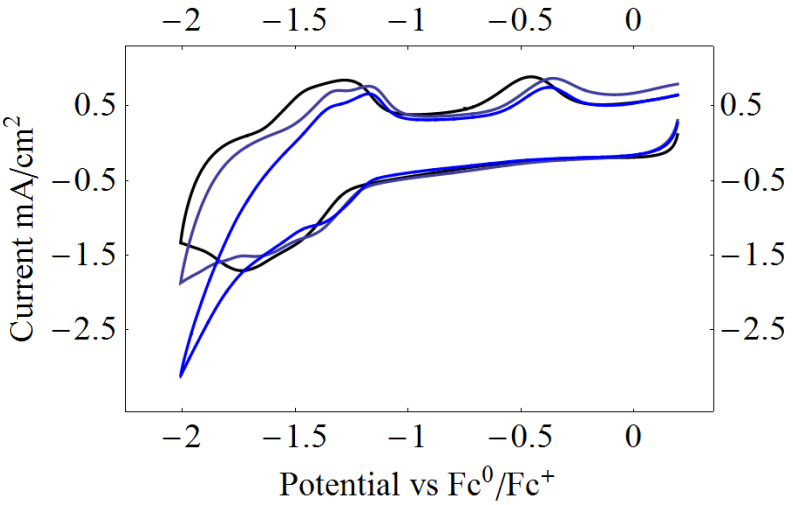

Figure 2.10 Cyclic voltammetry of immobilized 5 under Ar (black), with .4mM TFE (gray), and ,4mM trifluoroethanol under CO_2 (blue).

X-Ray Photoelectron Spectroscopy of Immobilized Complexes

The functionalized electrodes were then interrogated by X-ray photoelectron (XP) spectroscopy. A blank Ketjen black electrode shows features corresponding to carbon, oxygen, and fluorine. After soaking in a dilute solution containing **3**, new signals were observed for ruthenium (Ru 3p), nitrogen (N 1s), and chlorine (Cl 2p). Similarly, following immobilization of **4**, new peaks were clearly observable that correspond to iridium (Ir 4f and 4s), nitrogen (N 1s), and chlorine (2p). XP spectra collected for electrodes soaked in solutions containing a pyrene-free analogue, [Cp*Ir(2,2´-bipyridyl)Cl]Cl did not show

observable signals for iridium. [xxvi] Thus, as we have found in prior cases, the pyrene moieties were required for immobilization of the metal complex.

In high-resolution XP data (Figure 2.11), only a single contribution was visible for **3** in the Ru 3p region, with $3p_{3/2}$ and $3p_{1/2}$ peaks centered at 462.9 and 485.0 eV, respectively. An area ratio of 2:1 fit well for these peaks, as expected from theory. The high-resolution data for the N 1s revealed a single contribution as well, centered at 400.3 eV. These peak positions were compared with a drop-cast sample of $[Ru(bpy)_3]Cl_2$ on HOPG. Both the Ru 3p region (signals centered at 462.8 and 485.2 eV) and N 1s (single signal at 400.6 eV) were virtually identical to immobilized **1**. Comparing the peak areas of N 1s to Ru 3p revealed an elemental ratio of 10.7 to 1. This is close to the expected ratio of 8 to 1, but suggested an additional contribution to the nitrogen content, perhaps arising from acetonitrile solvent. The chlorine:ruthenium ratio (from Cl 2p signals) was found to be 1.5:1, which is near the expected value of 2:1.

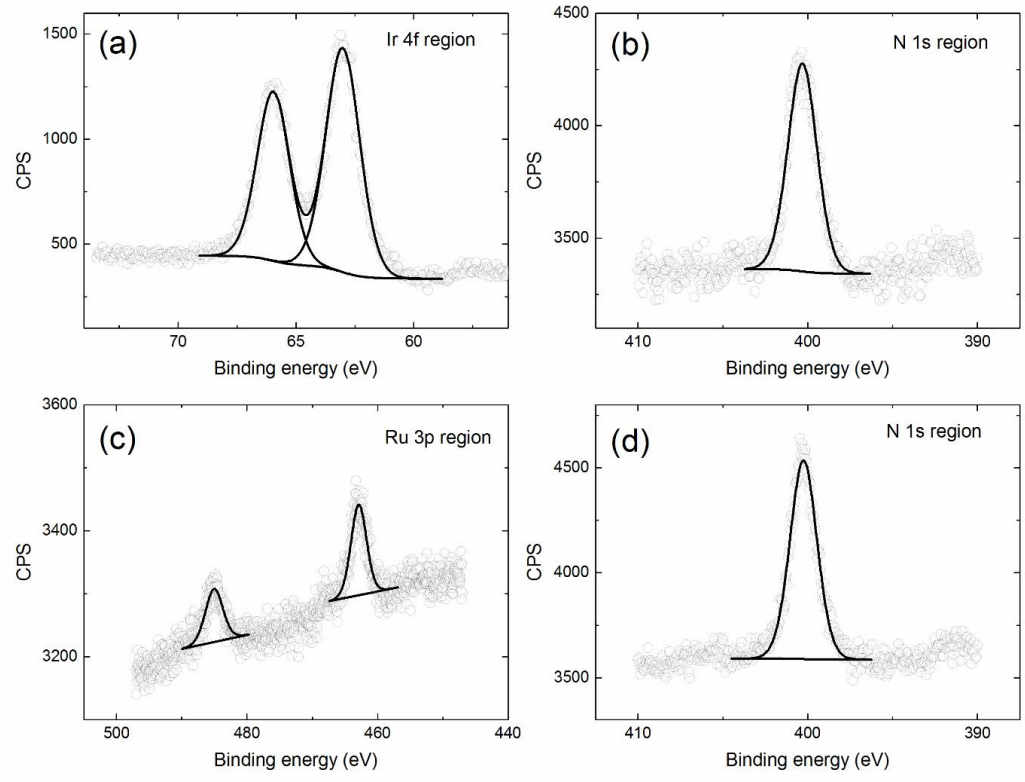

Figure 2.11 X-ray photoelectron spectra of the immobilized **3** (a and b) and **4** (c and d) in the Ir 4f region and N 1s region, and Ru 3p region.

High-resolution XP data for immobilized **4** suggest successful functionalization of the surface. Only a single contribution was apparent in the Ir 4f region, with peaks centered at 63.0 and 66 eV. An area ratio of 7:5 fit well for these peaks, as expected for f-electron peaks, and the spin-orbit splitting of ~3 eV matches well with values for iridium compounds. Only a single contribution was found in the N 1s region, as well, centered at 400.3 eV. These peak positions and ratios compare well with values obtained for drop-cast sample of **4** on HOPG. For example, the Ir 4f signals were found at 63.1 and 66.0 eV for **4**, while the N 1s signal was centered at 400.6 eV. The elemental ratio of nitrogen to iridium on carbon electrodes functionalized with **4** was found to be 6.5:1, again slightly higher than the expected stoichiometry. The ratio of chlorine to iridium was found to be 1.8:1, virtually identical to the expected value for two chloride counterions per iridium center.

Conclusion

We have synthesized and immobilized three pyrene-appended metal complexes on carbon electrodes: a ruthenium tris(bipyridyl) complex (**3**) and a bipyridyl complex of [Cp*Ir] (**4**) (Cp* = pentamethylcyclopentadienyl), and a manganese bipyridyl carbonyl complex (**5**). The results suggest that noncovalent interactions are suitable for obtaining new fundamental understanding of immobilized metal complexes and their reductive electrochemical properties. However, the stability of the noncovalent interaction is attenuated by negative electrode polarization; to the best of our knowledge, this effect has not been observed before. We have also found an earth abundant metal catalyst that is stable on the surface during continuous redox cyclic. Future studies will further investigate the products of the manganese catalyst and the attenuation of the non-covalent interaction, as they are relevant to the long-term use of noncovalent interactions in building integrated catalyst-electrodes for applications in production of solar fuel.

A p p e n d i x A

Supporting Information

General.

4,4′-Dimethyl-2,2′-bipyridine (GFS Chemicals), sulfuric acid (J.T. Baker), potassium dichromate, thionyl chloride, 1-Pyrenemethylamine hydrochloride (Sigma-Aldrich), $[Ru(bpy)_3]Cl_2$ (Sigma-Aldrich), ruthenium chloride hydrate, and iridium chloride hydrate (Pressure Chemical Co.) were used as received. were used as received. Acetonitrile (J.T. Baker) was dried using a Grubbs-type solvent purification system (Pure Process Technology/Glass Contour). 2,2′-Bipyridine-4,4′-dicarboxylic acid, $[Cp^*RhCl_2]_2$, [Cp*Rh(phen)Cl]Cl (**3**), and $Re(bpy)(CO)_3Cl$ (**4**) were prepared according to the literature. NMR spectra were recorded at room temperature on 300 or 500 MHz Varian spectrometers and referenced to the residual solvent peak (δ in ppm and *J* in Hz). Mass spectra were obtained with a PE SCIEX API 365 triple quadrupole spectrometer, and UV-vis spectra were obtained with an Agilent 8453 UV-Vis Spectrophotometer.

$N^{4,4'}$-bis(1-pyrenylmethyl)-[2,2′-dipyridyl]-4,4′-dicarboxamide (**P**).

The acid chloride of 2,2′-bipyridine-4,4′-dicarboxylic acid was prepared by refluxing 0.37 g (1.5 mmol) of the bipyridine-carboxylic acid in 15 mL of neat thionyl chloride for 8 h. Remaining thionyl chloride was removed under vacuum. In a separate flask, 0.8 g (3 mmol) of 1-pyrenemethylamine hydrochloride were combined with 150 mL of dry acetonitrile and 0.9 mL of 1,8-diazabicyclo[5.4.0]undec-7-ene (ca. 4 equivalents). The resulting solution was transferred to the solid bipyridine-acid chloride via cannula. The mixture was stirred for 12 h at room temperature, at which time 20 mL of saturated sodium bicarbonate and 130 mL deionized water were added to form a beige precipitate. The precipitate was collected using vacuum filtration and washed three times with 10 mL portions of deionized water. The precipitate was dried under vacuum to give 0.85 g (85%) of an off-white solid. ^{1}H NMR (300 MHz, DMSO-d_6) δ 5.26-5.28 (d, J= 5.27Hz, 4H), 8.05-8.17 (m, 9H), 8.26-8.32 (m, 9H), 8.49-8.52 (d, J= 8.51Hz, 2H), 8.83-8.85 (d, J= 8.84Hz, 2H), 8.85 (s 2H), 9.72 (s, 2H). ^{13}C

NMR (126 MHz, DMSO-d_6) δ 164.6, 155.5, 150.1, 142.7, 132.4, 130.8, 130.3, 130.2, 128.2, 127.7, 127.4, 127.1, 127.0, 126.3, 125.3, 125.2, 124.8, 124.1, 123.9, 123.2, 122.1, 118.3, 41.3. ESI-MS (positive) m/z: found 671.3 (**1** + H^+).

[(η^5-C_5Me_5)Rh(P)Cl]Cl (1)

A portion of $[Cp^*RhCl_2]_2$ (100 mg, 0.162 mmol) was dissolved in 20 mL of acetonitrile. A portion of **P** (150 mg, 0.338 mmol) was added to this solution, and following reflux for 24 hours at 60°C under argon, a yellow precipitate formed. The precipitate was filtered, and the solid redissolved in dichloromethane and filtered once more. A portion of diethyl ether was added to precipitate the product, which was then collected and dried under vacuum. ^{1}H NMR (300MHz, DMSO-d_6) δ 1.64 (s, 15H), 5.30-5.32 (d, 4H) 8.05-8.17 (m, 9H), 8.24-8.32 (m, 9H), 8.46-8.49 (d, 2H), 9.10-9.12 (d, 2H), 9.13 (s, 2H), 9.96 (s, 2H). ^{13}C NMR (126 MHz, DMSO-d_6) δ 162.8, 154.3, 153.0, 144.3, 131.9, 130.8, 130.30, 130.26, 128.2, 127.8, 127.4, 127.2, 126.9, 126.4, 126.3, 125.4, 125.3, 124.8, 124.1, 123.9, 123.2, 121.7, 97.4 (d, *J*=25 Hz, Cp* ring), 41.5, 8.4 (Cp* methyl). ESI-MS (positive) m/z: found 943.3 (**2** – Cl).

[Re(P)(CO)$_3$Cl] (2)

[Re(CO)$_5$Cl] (.50 g, .138 mmol) was dissolved in 20 mL of toluene. To this solution, a portion of **P** (.83g, .187 mmol) was added. After refluxing for 24 hours at 110°C under argon, the solution was filtered to give an orange solid. The solid material was redissolved in THF before being filtered once more to remove free **1**. The solution was then concentrated by rotary evaporation. 30 mL of diethyl ether was added to the solution and the product was filtered off as an orange precipitate. The precipitate was then collected and dried under vacuum before being stored. ^{1}H NMR (300 MHz, DMSO-d_6) δ 5.32-5.34 (d, J= 5.33Hz, 4H) 8.07-8.18 (m, J= 5.27Hz, 9H), 8.26-8.33 (m, 9H), 8.46-8.49 (d, J= 8.48Hz, 2H), 9.13 (s, 2H), 9.18-9.20 (d, J= 9.19Hz, 2H), 9.92 (s, 2H). ^{13}C NMR (126 MHz, DMSO-d_6) δ 163.1, 155.7, 153.8, 144.3, 131.8, 130.8, 130.3, 130.3, 128.3, 127.8, 127.4, 127.3, 126.9, 126.4, 125.8, 125.4, 125.4, 124.8, 124.1, 123.9, 123.1, 122.4, 41.5. ESI-MS (positive) m/z: found 941.2 (**3** – Cl^-).

[Ru(P)(4,4'-dimethyl-2,2'-bipyridine)$_2$]Cl$_2$ (3)

A portion of [Ru(Cl)$_2$(4,4'-dimethyl-2,2'-bipyridine)$_2$]Cl$_2$ (0.50 g, 1.77 mmol) was dissolved in dimethylformamide (25 mL). To this, **P** (1.25 g, 1.80 mmol) was added and the solution was refluxed for 24 hours. The product was precipitated by addition of diethyl ether (100 mL) and collected by filtration. The solid was then dissolved in hot dichloromethane and the resulting solution filtered to collect the remaining solid. The solid was dissolved in a minimum of methanol, and diethyl ether added until a precipitate began to form. The solution was then cooled in an ice bath; after cooling for one hour, the precipitate was collected by vacuum filtration. This process was repeated twice. The final precipitate was then collected and dried under vacuum (95 mg, 4.4%) before being stored. ^{1}H NMR (300 MHz, Methanol-d_4) δ 9.09 (s, 2H), 8.52-8.54 (d, J = 5.2 Hz, 4H), 8.37-8.40 (d, J = 9.2 Hz, 2H), 8.26 – 8.01 (m, 20H), 7.94-7.96 (d, J = 5.8 Hz, 2H), 7.85 – 7.84 (d, 2H), 7.50-7.56 (dd, J = 11.2, 5.7 Hz, 4H), 7.29-7.31 (d, J = 5.9 Hz, 2H), 7.19-7.20 (d, J = 5.6 Hz, 2H), 5.33 (s, 4H), 2.51-2.56 (d, J = 14.8 Hz, 12H). ESI-MS (positive) m/z: found 570.18 (**1** + H+). UV/Vis (DMF): λ_{max} (ε)=326 (24793), 340 (26813), 470 nm (8448 L mol^{-1} cm^{-1})

[(η^5-C$_5$Me$_5$)Ir(P)Cl]Cl (4)

A portion of [Cp*IrCl$_2$]$_2$ (0.10 g, 0.125 mmol) was dissolved in toluene (40 mL). A portion of **P** (0.175 g, 0.261 mmol) was added to this solution, and after refluxing for 24 hours under argon, a yellow precipitate formed. This precipitate was separated by filtration, and then redissolved in dichloromethane. The insoluble remaining material was filtered off and discarded before addition of a portion of diethyl ether to precipitate the product. The product was collected and dried under vacuum to yield a yellow solid (0.195 g, 80%). ^{1}H NMR (300 MHz, DMSO-d_6) δ 10.06 (s, 2H), 9.35 (s, 2H), 9.10-9.08 (d, J = 5.8 Hz, 2H), 8.52-8.49 (d, J = 9.1 Hz, 2H), 8.31 – 8.04 (m, 18H), 5.32-5.30 (d, J = 4.9 Hz, 4H), 1.62 (s, 15H). ^{13}C NMR (126 MHz, dmso) δ 163.03, 155.72, 153.18, 144.55, 132.25, 131.21, 130.74, 130.69, 128.61, 128.20, 127.79, 127.65, 127.36, 126.77, 125.83, 125.68, 125.18,

124.49, 124.31, 123.61, 90.14, 89.68, 41.93, 8.54. ESI-MS (positive) m/z: found 1033.34 (**2** + H+)

[Mn(*P*)(CO)$_3$Cl] (5)

[Mn(CO)$_5$Cl] (0.14 g, 0.509 mmol) was dissolved in 50 mL of DCM. To this solution, a portion of **P** (0.242 g, 0.363 mmol) was added. After refluxing for 24 hours under argon, the solution was filtered to give an orange solid. The solid material was redissolved in hot hexane before being filtered once more to remove free **P**. The solution was then concentrated by rotary evaporation. A portion of diethyl ether was added to the solution and the product was filtered off as an orange precipitate. The precipitate was then dried under vacuum to yield an orange solid 0.393 g (78%). ^{1}H NMR (300 MHz, DMSO-d_6) δ 5.26-5.28 (d, J=5.27Hz, 4H), 8.01 – 8.19 (m, 9H), 8.23-8.31 (m, 9H), 8.44-8.47 (d, J = 9.1Hz, 2H), 9.02 (s, 2H), 9.34-9.36 (d, J = 5.6Hz, 2H), 9.84 (s, 2H).

Carbon electrode preparation

Blocks of highly-oriented pyrolytic graphite (HOPG) carbon (GraphiteStore.com, Buffalo Grove, Ill.) were cleaned by sanding the basal plane with 600 grit silicon carbide paper, followed by sonication in water and methanol for 30 min each. The blocks were then rinsed with an additional portion of methanol before drying in air.

A suspension of Ketjen black was prepared by grinding 40 mg of the commercial material (EC600JD, AkzoNobel) with a mortar and pestle. The resulting powder was then combined with 5 mL *N*-methylpyrrolidone, 10 mg poly(vinylidene fluoride) (Sigma-Aldrich), and 0.75 g of Triton-X 100 and sonicated for 3 hours (VWR Aquasonic 150D).

To deposit the carbon black on the clean basal-plane surface of HOPG, the surface was first wet with acetonitrile, and then 10 μL per cm^2 of the carbon black suspension was added via pipette. The electrode was allowed to dry in ambient air for 15 min before transferring to an oven at 70^{o}C for 4 hours.

Electrochemistry

Electrochemical measurements were made with a Gamry Reference 600 potentiostat/galvanostat using a standard three-electrode configuration. For all experiments, the supporting electrolyte was 0.1 M fbutylammonium hexafluorophosphate (Fluka, electrochemical grade). In typical cyclic voltammetry measurements of immobilized complexes, the working electrode consisted of a 1 cm^2 block of HOPG prepared with carbon black on the basal plane as described above. The electrode was secured in a custom-made Teflon cell with an O-ring seal used to define the geometric area of the electrode (0.28 cm^2). The counter electrode was a Pt wire, and a silver wire immersed in a solution of 0.1 M NBu_4PF_6 served as a quasi-reference electrode. This quasi-reference was separated from the main working solution by a Vycor frit (Bioanalytical Systems, Inc.). The ferrocenium/ferrocene couple was used as an external reference in all experiments to calibrate potentials. Voltammetry collected for solution-soluble redox couples was obtained at a basal-plane HOPG working electrode electrode (surface area: 0.09 cm^2). A Pt wire served as the counter electrode, with a silver wire reference as described above.

Controlled-potential electrolysis coupled to product detection was carried out with a standard three-electrode configuration in a custom two-compartment air-tight cell. The working electrode consisted of a 10 cm^2 block of HOPG prepared with carbon black as described above. The reference and counter electrodes were as described above. The volume of solution held by the cell in total was 70 mL, with 100 mL of total headspace volume.
In a typical experiment for hydrogen gas detection, the cell was prepared in a nitrogen-filled glovebox with a 5 mM tosic acid solution in electrolyte. Following 1.25 hr of electrolysis, headspace gas was analysed for dihydrogen content. No other reduction products were detected.

In a typical experiment for CO gas detection, the cell was prepared in a nitrogen-filled glovebox with electrolyte. Then, the cell was removed from the glovebox and purged with CO_2 for 45 minutes before initiation of electrolysis. Following 1.25 hr of electrolysis, headspace gas was analyzed for CO content.

Gas chromatography

Gas analysis for the controlled-potential electrolyses was performed with an Agilent 7890A gas chromatograph with separate columns for analysis of hydrogen gas and nitrogen, oxygen, carbon dioxide, carbon monoxide, hydrogen disulfide, methane, ethane, ethylene, and ethyne. Each column was calibrated with standard gas mixtures to obtain quantitative data.

Minimal oxygen was detected in the headspace samples. As expected, large quantities of nitrogen and carbon dioxide were found in the runs for hydrogen production and CO production, respectively.

X-ray photoelectron spectroscopy.

XP data were collected using a Kratos AXIS Ultra system. The sample chamber was kept at $<5 \times 10^{-9}$ torr and ejected electrons were collected at an angle of 90° from the surface normal. The excitation source was Mg Kα radiation. Survey scans were performed to identify the elements on the surface of the carbon electrodes, while high resolution spectra were obtained and examined for specific elements. The XPS data were analyzed using the program Computer Aided Surface Analysis for X-ray Photoelectron Spectroscopy (CasaXPS). All XPS signals reported here are binding energies and are reported in eV. Ordinate axes are plotted as counts-per-second (CPS); these are arbitrary units. Backgrounds were fit with standard Shirley or linear backgrounds, as needed. Element peaks were fit with a standard Gaussian-Lorentzian line shape. The data were best fit with a single contribution in every case, and fits were constrained only based on peak area from theory

BIBLIOGRAPHY

[i] Gray, H. B. *Nature.*, **2009** *1*, 7.

[ii] Dempsey, J. L.; Brunschwig, B. S.; Winkler, J. R.; Gray, H. B. *Acc. Chem. Res.,* **2009**, *42*, 1995-2004.

[iii] Lewis, N. S.; Nocera, D. G. *Proc. Nat. Acad. Sci.* **2006**, *103*, 15729-15735.

[iv] Lattimer, J. R. C.; Blakemore, J. D.; Sattler, W.; Gul, S.; Chatterjee, R.; Yachandra, V. K.; Yano, J.; Brunschwig, B. S.; Lewis, N. S.; Gray, H. B. *Dalton Trans.* **2014**, *43*, 15004-15012.

[v] Schley, N. D.; Blakemore, J. D.; Subbaiyan, N. K.; Incarvito, C. D.; D'Souza, F.; Crabtree, R. H.; Brudvig, G. W. *J. Am. Chem. Soc.* **2011**, *133*, 10473-10481.

[vi] Katz, E. *J. Electroanal. Chem.* **1994**, *365*, 157-164.

[vii] Mann, J. A.; Rodríguez-López, J.; Abruña, H. D.; Dichtel, W. R. *J. Am. Chem. Soc.* **2011**, *133*, 17614-17617.

[viii] Tran, P. D.; Le Goff, A.; Heidkamp, J.; Jousselme, B.; Guillet, N.; Palacin, S.; Dau, H.; Fontecave, M.; Artero, V. *Angew. Chem. Int. Ed.* **2011**, *50*, 1371-1374.

[ix] Lee, C. W.; Gray, H. B.; Anson, F. C.; Malmstroem, B. G. *J. Electroanal. Chem. Interfacial Electrochem.* **1984**, *172*, 289-300.

[x] Udit, A. K.; Hill, M. G.; Bittner, V. G.; Arnold, F. H.; Gray, H. B. *J. Am. Chem. Soc.* **2004**, *126*, 10218-10219.

[xi] Giroud, F.; Milton, R. D.; Tan, B.-X.; Minteer, S. D. *ACS Catalysis* **2015**, *5*, 1240-1244.

[xii] Kölle, U.; Grützel, M. *Angew. Chem. Int. Ed. Engl.* **1987**, *26*, 567-570. (b) Kölle, U.; Kang, B. S.; Infelta, P.; Comte, P.; Graetzel, M. *Chem. Ber.* **1989**, *122*, 1869-1880.

[xiii] Hawecker, J.; Lehn, J. M.; Ziessel, R. *J. Chem. Soc., Chem. Commun.* **1983**, 536-538. (b) Hawecker, J.; Lehn, J. M.; Ziessel, R. *J. Chem. Soc., Chem. Commun.* **1984**, 328-330. (c) Hawecker, J.; Lehn, J. M.; Ziessel, R. *Helv. Chim. Acta* **1986**, *69*, 1990-2012.

[xiv] Kaim, W.; Reinhardt, R.; Waldhoer, E.; Fiedler, J. *J. Organomet. Chem.* **1996**, *524*, 195-202.

[xv] (a) Bard, A. J.; Faulkner, L. R. *Electrochemical Methods: Fundamentals and Applications*; 2nd ed.; Wiley: Hoboken, NJ, 2001. (b) Saveant, J.-M. *Elements of Molecular and Biomolecular Electrochemistry*; Wiley: Hoboken, NJ, 2006.

[xvi] (a) Smieja, J. M.; Kubiak, C. P. *Inorg. Chem.* **2010**, *49*, 9283-9289. (b) Sullivan, B. P.; Meyer, T. J. *Organometallics* **1986**, *5*, 1500-1502.

[xvii] Caix, C.; Chardon-Noblat, S.; Deronzier, A. *J. Electroanal. Chem.* **1997**, *434*, 163-170.

[xviii] Simon, J. A.; Curry, S. L.; Schmehl, R. H.; Schatz, T. R.; Piotrowiak, P.; Jin, X.; Thummel, R. P. *J. Am. Chem. Soc.* **1997**, *119*, 11012-11022.

[xix] Ozawa, H.; Kuroiwa, K.; Hasegawa, T.; Haga, M.-a. *Chem. Lett.* **2013**, *42*, 1059-1061.

[xx] Ding, S.-N.; Shan, D.; Cosnier, S.; Le Goff, A. *Chem. Eur. J.* **2012**, *18*, 11564-11568.

[xxi] Li, S.; Zhong, X.; Yang, H.; Hu, Y.; Zhang, F.; Niu, Z.; Hu, W.; Dong, Z.; Jin, J.; Li, R.; Ma, J. *Carbon* **2011**, *49*, 4239-4245.

[xxii] Agbo, P.; Heath, J. R.; Gray, H. B. *J. Phys. Chem. B* **2012**, *117*, 527-534.

[xxiii] Tokel, N. E.; Bard, A. J. *J. Am. Chem. Soc.* **1972**, *94*, 2862-2863.

[xxiv] Caix, C.; Chardon-Noblat, S.; Deronzier, A.; Ziessel, R. *J. Electroanal. Chem.* **1993**, *362*, 301-304.

[xxv] Kaim, W.; Reinhardt, R.; Waldhoer, E.; Fiedler, J. *J. Organomet. Chem.* **1996**, *524*, 195-202.

[xxvi] Ziessel, R. *J. Chem. Soc., Chem. Commun.* **1988**, 16-17.